# Environmental, phylogenetic, and palaeogeographic impact on relative septal thickness in Devonian ammonoids from Morocco

Ellen Langenberger Knudsen, Amane Tajika, Michael Hautmann & Christian Klug

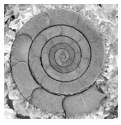

Building upon previous research, this study examines potential relationships between septal thickness in Devonian ammonoids from the Anti-Atlas of Morocco and isotopic proxy data from the literature for atmospheric $CO_2$, sea surface temperature, oceanic pH, and weathering ($\delta^{18}O$, $\delta^{13}C$, $\delta^{11}B$, $^{87}Sr/^{86}Sr$). Recent studies have demonstrated that various mollusc groups show some growth sensitive to environmental factors. Our results indicate no significant correlation between septal thickness and the examined proxies, except for significantly thinner septa in the genus *Phoenixites* following the environmental perturbations during the Kellwasser Event, which included anoxic conditions and possibly ocean acidification. This supports the hypothesis that a positive selection for reduced shell material occurred in response to changing seawater chemistry. Additionally, our results align with published data and may support a correlation between septal thickness and palaeolatitude. This study contributes to our understanding of the evolutionary impacts of environmental stressors such as ocean acidification on ammonoids and their adaptive strategies to changing environmental conditions. • Key words: Cephalopoda, palaeoecology, mass extinctions, ocean acidification, ontogeny.

Langenberger Knudsen, E., Tajika, A., Hautmann, M. & Klug, C. 2026. Environmental, phylogenetic, and palaeogeographic impact on relative septal thickness in Devonian ammonoids from Morocco. *Bulletin of Geosciences 101*(*2*), 191–220 (16 figures, 9 tables, electronic supplementary material). Czech Geological Survey, Prague. ISSN 1214-1119. Manuscript received September 19, 2025; accepted in revised form January 7, 2026; published online May 3, 2026; issued June 28, 2026.

*Ellen Langenberger Knudsen, Michael Hautmann & Christian Klug (corresponding author), Department of Palaeontology, Zurich University, Karl-Schmid-Strasse 4, 8006 Zürich; chklug@pim.uzh.ch • Amane Tajika, Hakubi Center for Advanced Research, Kyoto University, Yoshida-Honmachi, Sakyo-ku, Kyoto 606-8501, Japan & Graduate School of Human and Environmental Studies, Kyoto University, Yoshida Nihonmatsu-cho, Sakyo-ku, 606-8316 Kyoto, Japan & Division of Paleontology (Invertebrates), American Museum of Natural History, Central Park West 79th Street, New York, NY 10024, USA*

Studies of the fossil record allow us to assess the impact of environmental changes on the biosphere in deep time (Nätscher *et al.* 2021, Kiessling *et al.* 2025, Wang *et al.* 2025). Among the most crucial groups for such studies are ammonoids, an extinct clade of cephalopods. They emerged in the Early Devonian period (Klug *et al.* 2015b, Becker *et al.* 2019) and thrived for more than 300 million years until their eventual extinction at the end-Cretaceous mass extinction event (Tajika *et al.* 2018, 2020, 2023). During the time of their existence, ammonoids experienced numerous dramatic fluctuations in diversity due to several major extinction events (end-Devonian, end-Permian, and end-Triassic), as well as some smaller extinctions (*e.g.* Villier & Korn 2004, Korn *et al.* 2015, Becker *et al.* 2019). Due to their long time of existence (~ 340 Ma), wide geographical distribution, and great abundance, coupled with their high evolutionary rates (Sandoval *et al.* 2001), ammonoids are key fossils in the fields of biostratigraphy, evolution, biogeography, palaeoecology, and functional morphology (Klug *et al.* 2015a). The ammonoid conch consists of a body chamber containing the soft tissue, and a phragmocone, which is composed of individual chambers separated by septa and connected by the partially organic siphuncle (Klug *et al.* 2015a). The conch is primarily composed of aragonite (Kruta *et al.* 2014, Klug *et al.* 2015a, Janiszewska *et al.* 2018), a metastable polymorph of calcium carbonate that is 1.5 times more soluble than calcite (Morse & Mackenzie 1990). The shell is formed by biocalcification, an active and energy-intensive physiological process (Palmer 1992), which can be suppressed in a low pH-environment (Cohen & Holcomb 2009). Since the seawater is less saturated for aragonite than for calcite (Morse & Mackenzie 1990), aragonitic biomineralisers, like ammonoids, are

particularly susceptible to ocean acidification compared to calcitic biomineralisers (Hautmann 2006, Hautmann *et al.* 2008). Responses to ocean acidification vary in modern cephalopods (*e.g.* Borges *et al.* 2023). Some groups show difficulties with some calcified structures being negatively affected (*e.g.* statoliths: Maneja *et al.* 2011, Kaplan *et al.* 2013), while other groups show hypercalcification (internal shells: Gutowska *et al.* 2008, 2010; Dorey *et al.* 2013; Otjacques *et al.* 2020; Nätscher *et al.* 2021), particularly when not combined with starvation. Also, the calcifying process can be physiologically buffered versus unbuffered in different groups; ammonoids are usually assumed to form their shells under unbuffered conditions and hence can be considered more susceptible to be impacted by, *e.g.* ocean acidification (*e.g.* Bambach *et al.* 2002).

Various authors have argued that environmental factors influence septal spacing (within their life-time) in ammonoids as well as other cephalopods (Hewitt & Stait 1988, Kraft *et al.* 2008, Beck *et al.* 2021). There are also some potential evolutionary aspects of septal thickness; cephalopods (ammonoids are no exception) appear to usually prefer aragonite to construct their shell. However, during some times of calcite seas, some groups have convergently evolved bimineralic shells (*e.g.* Boggild 1930, De Baets & Munnecke 2018, Pohle *et al.* 2025).

Even though the septa are not in direct contact with the surrounding seawater, their formation is likely impacted by ocean acidification (Immenhauser *et al.* 2016). Under reduced seawater pH conditions, organisms may struggle to provide sufficient energy for maintaining the "normal" thickness of shell and in particular septa, which may have led to the formation of thinner septa (Weber *et al.* 2022). Ammonoids with thinner septa may have had an evolutionary advantage over species with thicker septa. The relative thickness of ammonoid septa might therefore reflect palaeoenvironmental conditions. In this context, we note that acidification may have affected the preservation of calcareous conchs (*e.g.* Trecalli *et al.* 2012, Hahn *et al.* 2014, Barclay *et al.* 2020), although we suggest that the effect was larger on the external parts, at least as long as the phragmocone had not been fully flooded. In this study, we build upon the research by Weber *et al.* (2022) by examining the septal thickness of Devonian ammonoids from the Anti-Atlas of Morocco.

A possible ocean acidification event in the Devonian occurred at the end of the Frasnian stage (Kiessling & Simpson 2011). For episodes, when ocean acidification appears more likely, such an environmental change in pH is still difficult to prove (*e.g.* Hönisch *et al.* 2012). Also, it appears that the potential Devonian ocean acidification differed from other instances of ocean acidification and rather may have been more regional as well as linked with other environmental changes (*e.g.* anoxia; Kiessling & Simpson 2013).

Our principal proxy data for Devonian seawater pH are published data on boron isotopes (Joachimski *et al.* 2005) and $pCO_2$ (Foster *et al.* 2017, Brugger *et al.* 2019). Additionally, we examined possible correlation between septal thickness and a variety of additional environmental proxies such as $\delta^{18}O$, $\delta^{13}C$, and $^{87}Sr/^{86}Sr$, which reflect palaeotemperature, intensity of the biological pump, and intensity of continental weathering, respectively. Finally, we examined the influence of palaeogeographical position and phylogeny on the septal thickness. The aim is to determine whether and how ocean chemistry affected ammonoids, and to evaluate whether the relative septal thickness of ammonoids can serve as a reliable palaeoecological proxy.

## Material and methods

### Morphometry

Over 200 Devonian ammonoids collected from the eastern Anti-Atlas of Morocco were cut, polished, and examined for their septal preservation. Out of this material, 65 specimens showed sufficient preservation and were selected for morphometric measurements (Tab. 1, Figs 1–5). For this study, the thickness of 1305 septa was measured. For each specimen, between four and 76 septa were measured (see the supplementary table). Per genus, between eight (*Mithraxites*) and 135 septa (*Cymaclymenia*) contributed to our dataset. Many of these specimens exhibit well-preserved septa throughout much of their ontogeny, although some have only a limited number of measurable septa. Nevertheless, all values of measurable septa were included in the analyses, because the data of all specimens belonging to the same genus is combined. As discussed in Weber *et al.* (2022), we assume that the recrystallization process does not significantly alter the septal thickness. Following the method of Weber *et al.* (2022), all ammonoids were polished until the siphuncle became visible in most whorls, minimizing deviations from the plane of symmetry. Only septa

**Figure 1.** Emsian ammonoids (for details see Tab. 1). • A, B – *Erbenoceras* sp.; A – PIMUZ 41645; B – PIMUZ 41644. • C, D – *Latanarcestes* sp.; C – PIMUZ 41647; D – PIMUZ 41646. • E–I, K, L – *Sellanarcestes* sp.; E – PIMUZ 41648; F – PIMUZ 41654; G – PIMUZ 41652; H – PIMUZ 41650; I – PIMUZ 41651; K – PIMUZ 41653; L – PIMUZ 41649. • J – *Achguigites tafilaltensis* Klug, 2002, PIMUZ 41655. • M–P – *Anarcestes* sp.; M – PIMUZ 41659; N – PIMUZ 41658; O – PIMUZ 41657; P – PIMUZ 41656. Scale bar = 1 cm.

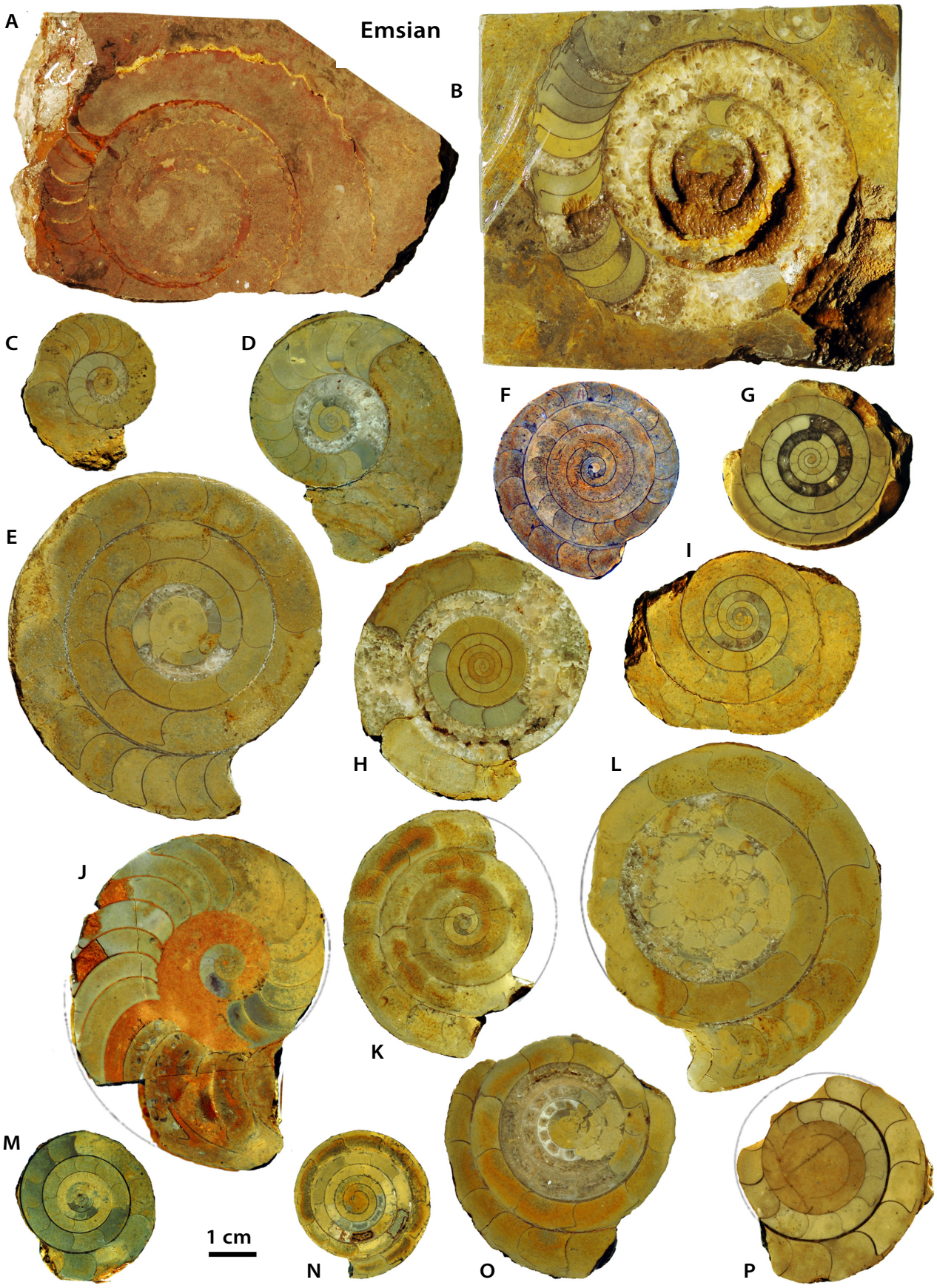
A
Emsian
B
C
D
F
G
E
I
H
L
J
K
M
1 cm
N
O
P

**Table 1.** Catalogue of all specimens used in this study. The collection number is the repository number of the Department of Palaeontology of the University of Zurich without the PIMUZ for brevity.

| Nr | Repository Nr. | Species | Family | Origin | Time Bin |
|---|---|---|---|---|---|
| 1 | 41708 | *Cymaclymenia* sp. | Cymaclymeniidae | Filon Douze | late Famennian |
| 2 | 41707 | *Cymaclymenia striata* | Cymaclymeniidae | Lambidia, Maider | late Famennian |
| 3 | 41706 | *Cymaclymenia striat*a | Cymaclymeniidae | Lambidia, Maider | late Famennian |
| 4 | 41705 | *Platyclymenia* sp. | Platyclymeniidae | Madene | late Famennian |
| 5 | 41704 | *Platyclymenia* sp. | Platyclymeniidae | Madene | late Famennian |
| 6 | 41703 | *Platyclymenia* sp. | Platyclymeniidae | Bou Tchratine | late Famennian |
| 7 | 41702 | *Sporadoceras muensteri* | Sporadoceratidae | Madene | late Famennian |
| 8 | 41701 | *Sporadoceras muensteri* | Sporadoceratidae | Madene | late Famennian |
| 9 | 41700 | *Sporadoceras muensteri* | Sporadoceratidae | Madene | late Famennian |
| 10 | 41699 | *Phoenixites* sp. | Tornoceratidae | Oued Ziz Taouz | early Famennian |
| 11 | 41698 | *Phoenixites* sp. | Tornoceratidae | Oued Ziz Taouz | early Famennian |
| 12 | 41697 | *Phoenixites* sp. | Tornoceratidae | Oued Ziz Taouz | early Famennian |
| 13 | 41696 | *Phoenixites* sp. | Tornoceratidae | Oued Ziz Taouz | early Famennian |
| 14 | 41695 | *Manticoceras* sp. | Gephuroceratidae | Bou Ifarherioun | Frasnian |
| 15 | 41694 | *Manticoceras* sp. | Gephuroceratidae | Bou Ifarherioun | Frasnian |
| 16 | 41693 | *Manticoceras* sp. | Gephuroceratidae | Bou Ifarherioun | Frasnian |
| 17 | 41692 | *Manticoceras* sp. | Gephuroceratidae | Bou Ifarherioun | Frasnian |
| 18 | 41691 | *Manticoceras* sp. | Gephuroceratidae | Bou Mais | Frasnian |
| 19 | 41690 | *Manticoceras* sp. | Gephuroceratidae | Bou Ifarherioun | Frasnian |
| 20 | 41689 | *Beloceras* sp. | Beloceratidae | Hamar Laghdad | Frasnian |
| 21 | 41688 | *Beloceras* sp. | Beloceratidae | Hamar Laghdad | Frasnian |
| 22 | 41687 | *Synpharciceras* sp. | Pharciceratidae | Jebel Mdouar | Givetian |
| 23 | 41686 | *Synpharciceras* sp. | Pharciceratidae | Jebel Mdouar | Givetian |
| 24 | 41685 | *Synpharciceras* sp. | Pharciceratidae | Jebel Mdouar | Givetian |
| 25 | 41684 | *Synpharciceras* sp. | Pharciceratidae | Jebel Mdouar | Givetian |
| 26 | 41683 | *Synpharciceras* sp. | Pharciceratidae | Jebel Mdouar | Givetian |
| 27 | 41682 | *Synpharciceras* sp. | Pharciceratidae | Jebel Mdouar | Givetian |
| 28 | 41681 | *Synpharciceras* sp. | Pharciceratidae | Jebel Mdouar | Givetian |
| 29 | 41680 | *Synpharciceras* sp. | Pharciceratidae | Jebel Mdouar | Givetian |
| 30 | 41679 | *Pharciceras* sp. | Pharciceratidae | Jebel Mdouar | Givetian |
| 31 | 41678 | *Pharciceras* sp. | Pharciceratidae | Jebel Mdouar | Givetian |
| 32 | 41677 | *Pharciceras* sp. | Pharciceratidae | Jebel Mdouar | Givetian |
| 33 | 41676 | *Pharciceras* sp. | Pharciceratidae | Jebel Mdouar | Givetian |
| 34 | 41675 | *Pharciceras* sp. | Pharciceratidae | Hamar Laghdad | Givetian |
| 35 | 41674 | *Agoniatites* sp. | Agoniatitidae | Filon Douze | Eifelian |
| 36 | 41673 | *Cabrieroceras* sp. | Cabrieroceratidae | Filon Douze | Eifelian |
| 37 | 41672 | *Cabrieroceras* sp. | Cabrieroceratidae | Hamar Laghdad | Eifelian |
| 38 | 41671 | *Diallagites* sp. | Werneroceratidae | Hamar Laghdad | Eifelian |
| 39 | 41670 | *Diallagites* sp. | Werneroceratidae | Filon Douze | Eifelian |
| 40 | 41669 | *Sobolewia* sp. | Sobolewiidae | Filon Douze | Eifelian |
| 41 | 41668 | *Subanarcestes* sp. | Sobolewiidae | Filon Douze | Eifelian |
| 42 | 41667 | *Subanarcestes* sp. | Sobolewiidae | Filon Douze | Eifelian |
| 43 | 41666 | *Fidelites* sp. | Agoniatitidae | Filon Douze | Eifelian |
| 44 | 41665 | *Fidelites clariondi* | Agoniatitidae | Filon Douze | Eifelian |
| 45 | 41664 | *Fidelites* sp. | Agoniatitidae | Jebel Mdouar | Eifelian |
| 46 | 41663 | *Fidelites* sp. | Agoniatitidae | Filon Douze | Eifelian |
| 47 | 41662 | *Fidelites* sp. | Agoniatitidae | Hamar Laghdad | Eifelian |
| 48 | 41661 | *Mithraxites* sp. | Parodoceratidae | Filon Douze | Eifelian |
| 49 | 41660 | *Crispoceras* sp. | Werneroceratidae | Hamar Laghdad | Eifelian |
| 50 | 41659 | *Anarcestes* sp. | Anarcestidae | Filon Douze | late Emsian |
| 51 | 41658 | *Anarcestes* sp. | Anarcestidae | Filon Douze | late Emsian |
| 52 | 41657 | *Anarcestes* sp. | Anarcestidae | Filon Douze | late Emsian |
| 53 | 41656 | *Anarcestes* sp. | Anarcestidae | Filon Douze | late Emsian |
| 54 | 41655 | *Achguigites tafilaltensis* | Agoniatitidae | Filon Douze | late Emsian |
| 55 | 41654 | *Sellanarcestes* sp. | Anarcestidae | Filon Douze | late Emsian |
| 56 | 41653 | *Sellanarcestes* sp. | Anarcestidae | Filon Douze | late Emsian |
| 57 | 41652 | *Sellanarcestes* sp. | Anarcestidae | Filon Douze | late Emsian |
| 58 | 41651 | *Sellanarcestes* sp. | Anarcestidae | Filon Douze | late Emsian |
| 59 | 41650 | *Sellanarcestes tenuior* | Anarcestidae | Filon Douze | late Emsian |
| 60 | 41649 | *Sellanarcestes tenuior* | Anarcestidae | Filon Douze | late Emsian |
| 61 | 41648 | *Sellanarcestes tenuior* | Anarcestidae | Filon Douze | late Emsian |
| 62 | 41647 | *Latanarcestes* sp. | Latanarcestidae | Filon Douze | late Emsian |
| 63 | 41646 | *Latanarcestes* sp. | Latanarcestidae | Filon Douze | late Emsian |
| 64 | 41645 | *Erbenoceras* sp. | Mimosphinctidae | Ouidane Chebbi | early Emsian |
| 65 | 41644 | *Erbenoceras* sp. | Mimosphinctidae | Filon Douze | early Emsian |

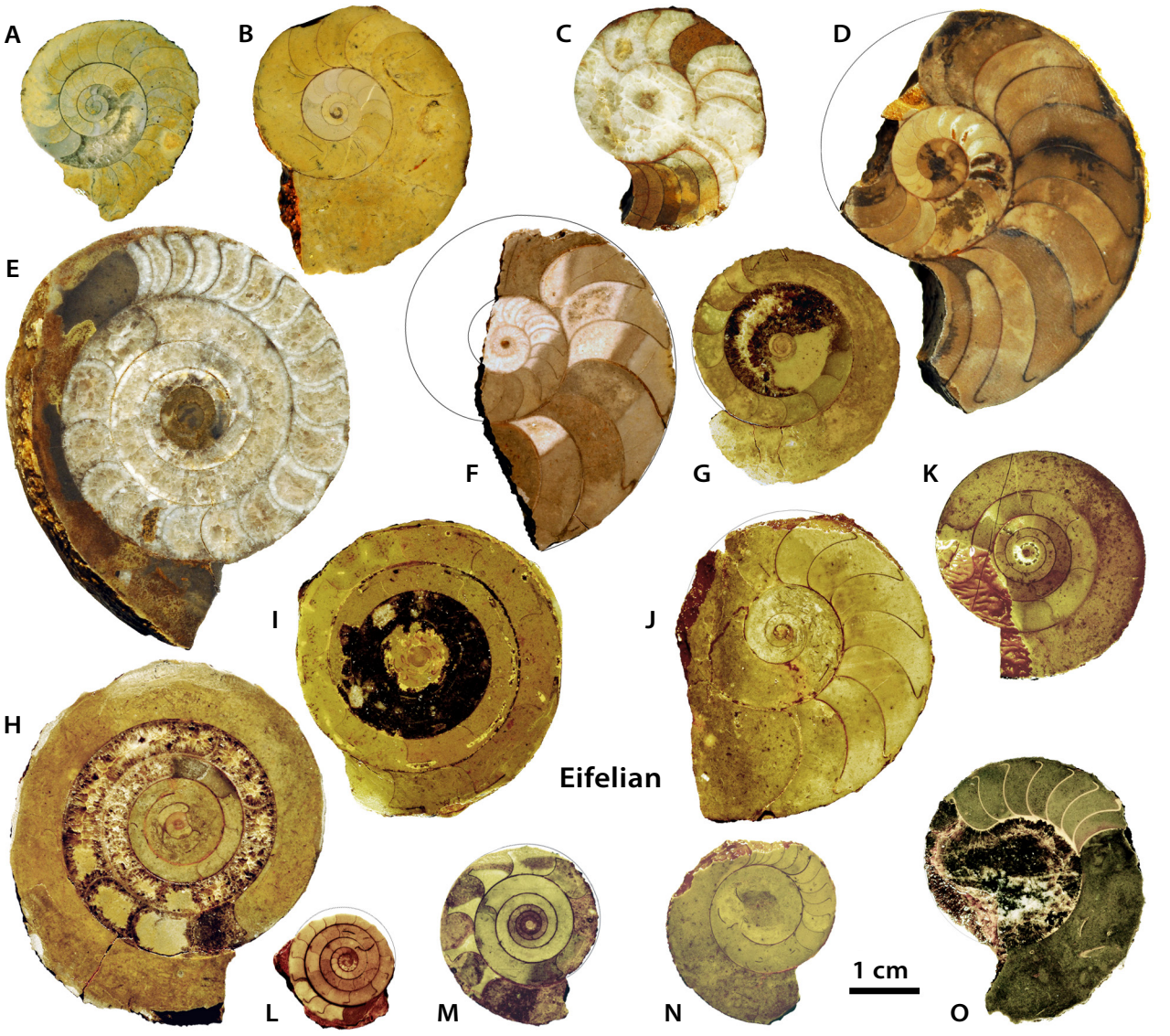


**Figure 2.** Eifelian ammonoids (for details see Tab. 1). • A–D, F – *Fidelites* sp.; A – PIMUZ 41666; B – PIMUZ 41664; C – PIMUZ 41665; D – PIMUZ 41662; F – PIMUZ 41663. • E – *Crispoceras* sp., PIMUZ 41660. • G, K – *Diallagites* sp.; G – PIMUZ 41671; K – PIMUZ 41670. • H, I – *Cabrieroceras* sp.; H – PIMUZ 41672; I – PIMUZ 41673. • J – *Agoniatites* sp., PIMUZ 41674. • L, M – *Subanarcestes* sp.; L – PIMUZ 41668; M – PIMUZ 41667. • N – *Sobolewia* sp., PIMUZ 41669. • O – *Mithraxites* sp., PIMUZ 41661.

oriented approximately perpendicular to the polished surface were measured to mitigate thickness-related biases linked with the inclination relative to the polished plane. High-resolution photographs were taken of all the cross-sections. Small specimens and specimens with well-preserved inner septa were additionally scanned with a Keyence microscope of the VHX-7000 series. The outer shell of slightly incomplete specimens was reconstructed using the Krita software (version 5.0.2) to allow for diameter measurements; these reconstructions are shown as very fine lines in the first five figures. All visible and sufficiently preserved septa as well as the diameter and whorl height were measured using ImageJ (version 1.53t). The morphometric measurements encompass the data of septal thickness, diameter, and whorl height of all visible and sufficiently preserved septa. To account for the diverse septal morphologies observed in ammonoids, Weber *et al.* (2022) measured the septa at the inner, middle, and outer portions. However, given the somewhat poor preservation and the substantial variation in inclination near the inner and outer portion of the septa in many of the specimens, only a single measurement at the middle portion was taken in this study. To minimize errors, each septum was measured at the point where the best preservation of the septum was given within the middle part of the septum, where the variation in thickness from dorsal to ventral is minimal (Fig. 6A, green part of septum) and the septal surface is perpendicular to the plane of symmetry. The

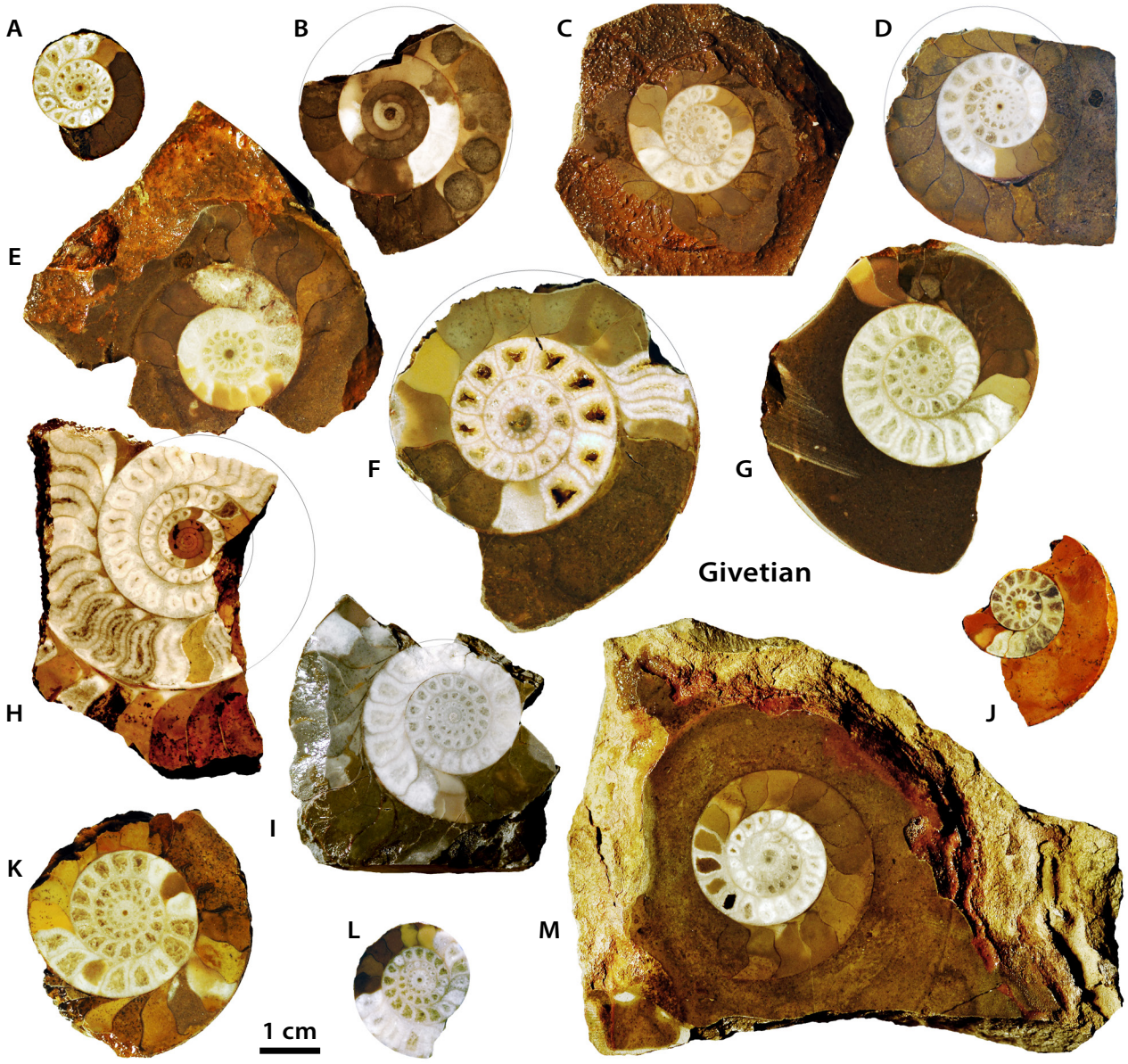


**Figure 3.** Givetian ammonoids (for details see Tab. 1). • A–C, E, F – *Pharciceras* sp.; A – PIMUZ 41679; B – PIMUZ 41678; C – PIMUZ 41677; D – PIMUZ 41685; E – PIMUZ 41676; F – PIMUZ 41675. • G–M – *Synpharciceras* sp.; G – PIMUZ 41682; H – PIMUZ 41681; I – PIMUZ 41684; J – PIMUZ 41686; K – PIMUZ 41683; L – PIMUZ 41687; M – PIMUZ 41680.

conch diameter was measured at the position of each septum. To measure the diameter, a line between the point at which the septum and outer shell connects and the coiling centre was drawn (Fig. 6A, red line), which was then extended to the edge of the outer shell on the opposite side (Fig. 6A, blue arrow). The length of the line was defined as the conch diameter. For the order Clymeniida (*Cymaclymenia* and *Platyclymenia*), where the siphuncle is located dorsally, the point on the dorsal shell closest to the septal neck was connected to the coiling centre (Fig. 6B, red line) and the line was extended on both sides to the inside of the ventral shell (Fig. 6B, blue arrows). Since the outer shell (or its calcitic replacement) is not preserved in all specimens, the measurement of the conch diameter does not include the outer shell (the connected points are on the inner side of the outer shell, *i.e.* the surface of the internal mould, even if replacement shell is present).

Errors in our measurements may have different origins. For example, if the specimen is cut slightly obliquely and thus not exactly in the plane of symmetry, this causes deviations from the accurate values. Also, the septal thickness is, in most cases, so low that these measurements already have a certain error, due to limited resolution of the photographs. To minimize the latter error, very thin

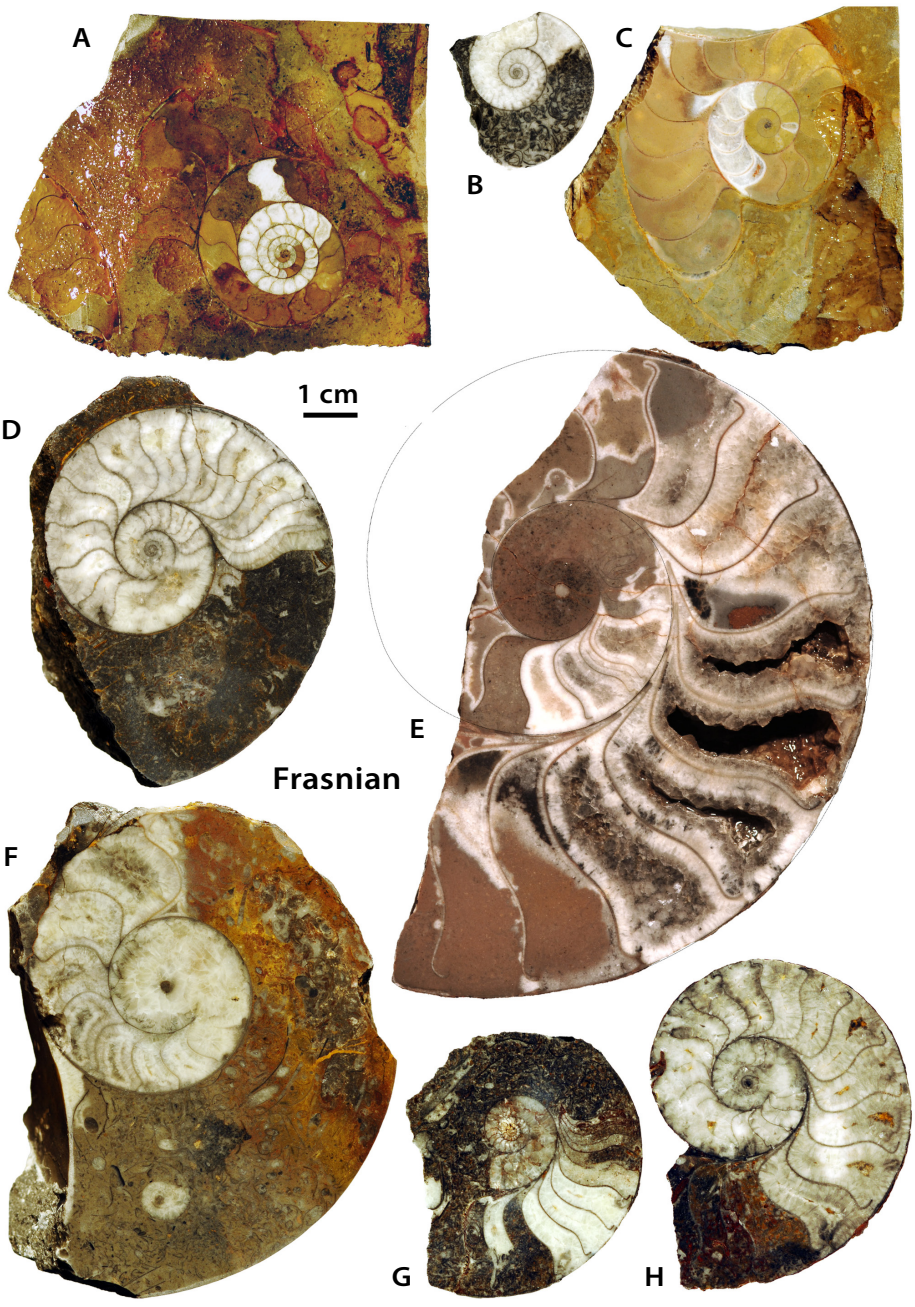


**Figure 4.** Frasnian ammonoids (for details see Tab. 1). • A, C – *Beloceras* sp.; A – PIMUZ 41689; C – PIMUZ 41688. • B, D–H – *Manticoceras* sp.; B – PIMUZ 41695; D – PIMUZ 41691; E – PIMUZ 41690; F – PIMUZ 41692; G – PIMUZ 41694; H – PIMUZ 41693.

septa were additionally photographed using a Keyence microscope to maximize the resolution and minimize the measurement error. To level out simple measurement errors to some degree, we employed the septal slope factor (SSF) introduced by Weber *et al.* (2022). The septal slope factor is the slope of the linear regression line of the conch diameter/septal thickness relationship; a higher septal slope factor indicates thicker septa. The septal slope factor accounts for the ontogenetic increase of septal thickness and allows us to compare septal thickness among different genera. The SSF was calculated by performing a linear regression with the conch diameter as the independent and the septal thickness as the dependent variable, using the slope of the linear regression as the comparative factor. The septal slope factor is useful as an indicator for septal thickness, when the measurements have a small error, and the linear regression line points to the origin. However, when the intercept of the linear regression significantly deviates from zero, it is possible to get two lines with the same slope, but a vastly different septal thickness for any given conch diameter (a parallel shift along the y-axis). This makes the septal slope factor susceptible to outliers in specimens with very few datapoints, which can lead to an extremely negative intercept and an exaggerated septal

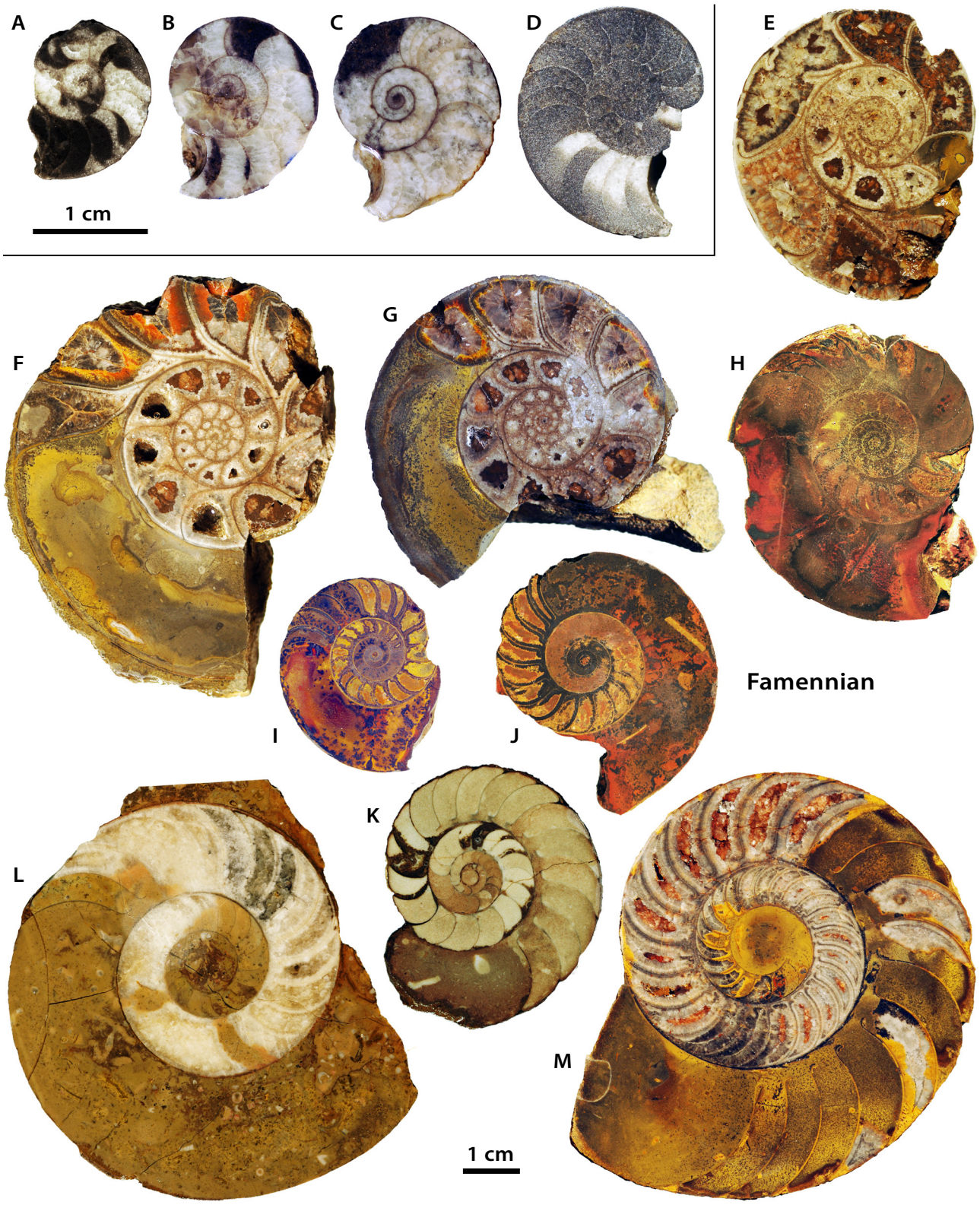


**Figure 5.** Famennian ammonoids (for details see Tab. 1). • A–D – *Phoenixites* sp.; A – PIMUZ 41699; B – PIMUZ 41698; C – PIMUZ 41697; D – PIMUZ 41696. • E–G – *Sporadoceras muensteri* (von Buch, 1832); E – PIMUZ 41702; F – PIMUZ 41700; G – PIMUZ 41701. • H–J – *Cymaclymenia striata* (Münster, 1832); H – PIMUZ 41706; I – PIMUZ 41708; J – PIMUZ 41707. • K–M – *Platyclymenia* sp.; K – PIMUZ 41705; L – PIMUZ 41703; M – PIMUZ 41704.

**Table 2.** All 21 genera examined in this study, together with (from left to right): adjusted septal slope factor (short: aSSF) and $R^2$ – value from linear regression (with y = septal thickness; x = conch diameter; Intercept = 0); septal slope factor (short: SSF), intercept and $R^2$ – value from linear regression (with y = septal thickness; x = conch diameter); suborder; time Bin. Visualization in Figures 7, 8.

| Genus | aSSF | $R^2$ | SSF | Intercept | $R^2$ | Suborder | Time Bin |
|---|---|---|---|---|---|---|---|
| *Cymaclymenia* | 0.0038 | 0.9209 | 0.0041 | −0.0052 | 0.8281 | Cyrtoclymeniina | late Famennian |
| *Platyclymenia* | 0.0044 | 0.9310 | 0.0050 | −0.0240 | 0.8378 | Clymeniina | late Famennian |
| *Sporadoceras* | 0.0050 | 0.9331 | 0.0054 | −0.0145 | 0.8275 | Tornoceratina | late Famennian |
| *Phoenixites* | 0.0015 | 0.8579 | 0.0007 | 0.0101 | 0.1639 | Tornoceratina | early Famennian |
| *Manticoceras* | 0.0053 | 0.9320 | 0.0046 | 0.0359 | 0.7355 | Gephuroceratina | Frasnian |
| *Beloceras* | 0.0041 | 0.9695 | 0.0037 | 0.0073 | 0.9315 | Gephuroceratina | Frasnian |
| *Synpharciceras* | 0.0051 | 0.9558 | 0.0045 | 0.0145 | 0.7256 | Pharcicerattina | Givetian |
| *Pharciceras* | 0.0045 | 0.9623 | 0.0039 | 0.0191 | 0.7607 | Pharcicerattina | Givetian |
| *Agoniatites* | 0.0052 | 0.9828 | 0.0054 | −0.0082 | 0.9643 | Agoniatitina | Eifelian |
| *Cabrieroceras* | 0.0037 | 0.9537 | 0.0047 | −0.0310 | 0.7492 | Anarcestina | Eifelian |
| *Diallagites* | 0.0031 | 0.9869 | 0.0032 | −0.0015 | 0.9223 | Anarcestina | Eifelian |
| *Sobolewia* | 0.0030 | 0.9875 | 0.0055 | −0.0451 | 0.3983 | Anarcestina | Eifelian |
| *Subanarcestes* | 0.0046 | 0.9860 | 0.0035 | 0.0157 | 0.9076 | Anarcestina | Eifelian |
| *Fidelites* | 0.0055 | 0.9453 | 0.0049 | 0.0173 | 0.8459 | Agoniatitina | Eifelian |
| *Mithraxites* | 0.0062 | 0.9935 | 0.0102 | −0.1091 | 0.6930 | Tornoceratina | Eifelian |
| *Crispoceras* | 0.0028 | 0.9919 | 0.0026 | 0.0081 | 0.6500 | Anarcestina | Eifelian |
| *Anarcestes* | 0.0045 | 0.9462 | 0.0049 | −0.0112 | 0.7905 | Anarcestina | late Emsian |
| *Achguigites* | 0.0044 | 0.9729 | 0.0047 | −0.0086 | 0.9745 | Agoniatitina | late Emsian |
| *Sellanarcestes* | 0.0035 | 0.9437 | 0.0029 | 0.0251 | 0.7956 | Anarcestina | late Emsian |
| *Latanarcestes* | 0.0044 | 0.9657 | 0.0036 | 0.0206 | 0.8959 | Agoniatitina | late Emsian |
| *Erbenoceras* | 0.0033 | 0.9321 | 0.0047 | −0.0707 | 0.9352 | Agoniatitina | early Emsian |

slope factor. To eliminate this problem, we performed the same linear regression with the conch diameter as the independent and the septal thickness as the dependent variable, while additionally setting the intercept equal to zero, thus forcing the linear regression line through the origin. The new slope, the adjusted septal slope factor (aSSF), is a better indicator for the septal thickness, especially when the error of measurement is significant. In this study, we examine both the SSF and the aSSF (Tab. 2, Figs 7, 8). Both factors were used for statistical analyses to investigate the impact of environmental parameters and to visualize differences between ammonoid taxa and thus the influence of phylogenetic relationships on the septal thickness. The statistical analyses were carried out in the statistical environment R (version 4.2.3). The ggpubr R package was used for ggplot2-based data visualisation. All specimens are kept in the collection of the Department of Palaeontology of the University of Zurich with the abbreviation PIMUZ.

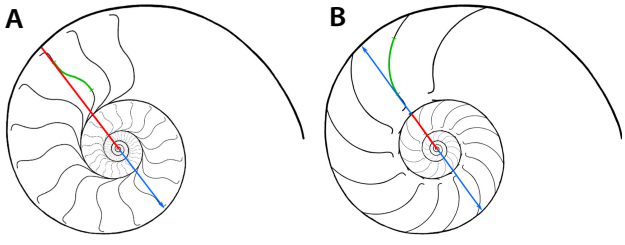


**Figure 6.** Measurements. • A – longitudinal section representing most Devonian ammonoids. • B – longitudinal section representing the order Clymeniida; green segments: part of septum, wherein the septal thickness was measured; red lines: connection between the coiling centre and point on ventral shell (A) / dorsal shell (B) closest to the septal bent; blue arrows: extensions of red lines to the outer shell; conch diameter at a specific septum = red line + blue arrow(s). Further information in the chapter Morphometry.

## Analysis of environmental parameters

Quantitative data of the following abiotic factors was gathered from the literature: atmospheric $CO_2$ concentration (Foster *et al.* 2017, Brugger *et al.* 2019), isotopic sea surface temperature (Joachimski *et al.* 2009, Brugger *et al.* 2019), $\delta^{18}O_{brachiopods}$ (van Geldern 2004, Joachimski *et al.* 2009, Brugger *et al.* 2019), $\delta^{18}O_{conodonts}$ (Grossman

& Joachimski 2020), $\delta^{13}C_{brachiopods}$ and $^{87}Sr/^{86}Sr_{brachiopods}$ (van Geldern 2004), $\delta^{11}B_{brachiopods}$ (Joachimski *et al.* 2005). Wherever possible, the original proxy data was used for the statistical tests. For correlation tests between the adjusted septal slope factor and abiotic parameters, a single value from each abiotic factor was calculated for each genus (Tab. 3, for further information see the correlation of timescales section below). Following the methodology of Weber *et al.* (2022), the aSSF and the abiotic factors were tested for constantly increasing or decreasing trends by performing the Mann-Kendall test (non-parametric test for monotonic trend detection; Helsel & Frans 2006) (Tab. 4). Since all the data is given in the form of time series, it is not surprising that a significant number of abiotic factors show a *p*-value smaller than the critical value of 0.05, thus the null-hypothesis must be rejected, and a monotonic trend is assumed for those factors. The Shapiro-Wilk test was performed on the adjusted septal slope factor and all abiotic factors as well, to test if they follow a normal distribution (Shapiro & Wilk 1965) (Tab. 4). Since most *p*-values are significantly lower than 0.05 a non-normal distribution of the data must be assumed. The aSSF and the $\delta^{11}B$ isotope have a *p*-value above 0.05. (0.84 and 0.62). This means that, in case of a normal distribution of the data, there is an 84% and 62% chance of obtaining the measured data. Since in these two factors, the number of datapoints is not very high and the chance is not above 95% (*p*-value > 0.95), we do not assume a normal distribution in these two factors. To test for homogeneity of variances with non-normally distributed factors, the Fligner-Killeen test was applied (Fligner & Killeen 1976) (Tab. 5). Under consideration of the degrees of freedom, returned by the test, the significance of the $\chi^2$-values can be assessed

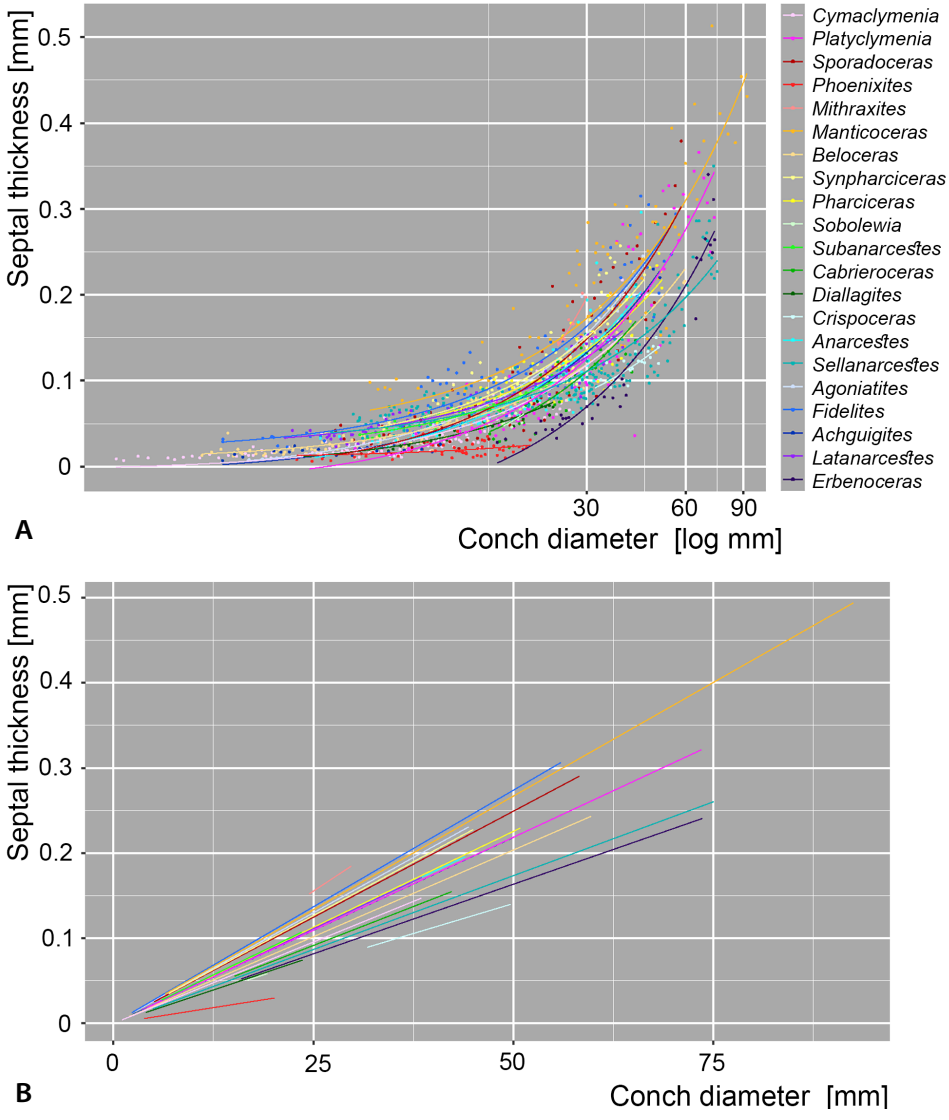


**Figure 7.** Biplots of septal thickness of all genera. • A – semilogarithmic biplot of septal thickness versus conch diameter at the measured septa position for all ammonoid genera. The lines represent the linear regression lines for each ammonoid genus. • B – linear biplot of the same data, displaying linear regression lines with intercept = 0, and slope = adjusted septal slope factor.

from published tables on chi-square probabilities (*e.g. https://people.richland.edu /james/lecture/m170/tbl-chi.html*). The $\chi^2$-values from the test are all lower than the critical values, thus the null-hypothesis ($H_0$) cannot be rejected, and the variances are assumed to be homogenous. Alternatively, the same conclusion can be drawn from the fact that all *p*-values returned by the test are significantly greater than 0.05. Finally, the Spearman's Rank correlation coefficient was calculated (Spearman 1904). To correct for the increased risk of a false positive, due to the data being expressed as a time series, the generalized differencing of timeseries by Graeme T. Lloyd (*http://www.graemetlloyd.com/methgd.html*) was performed. The correlation coefficient ρ can take on values from −1 to 1, where −1 and 1 indicate a strong negative or positive correlation and 0 implies no correlation. Since all correlation coefficients ρ are between −0.4 and 0.4 and the *p*-values are greater than the critical value of 0.05, no statistically significant correlation can be inferred (Tab. 6). Since we performed multiple statistical tests on the same dataset, we need to correct for false positives (random events that falsely appear significant). For this, we used the false discovery rate (FDR) (Rouam 2013), which takes the *p*-values and the number of tests as input and yields corrected *p*-values [p (FDR) in Tabs 4–6]. After the correction, all statistical tests still show the same significance as before (*p*-values smaller than the critical value of 0.05 are still smaller and *vice versa*).

## Adjustment of timescales

The timescale used in this study is taken from The Geologic Time Scale 2020 (GTS2020, Becker *et al.* 2020). The timescales, by which the absolute age of the

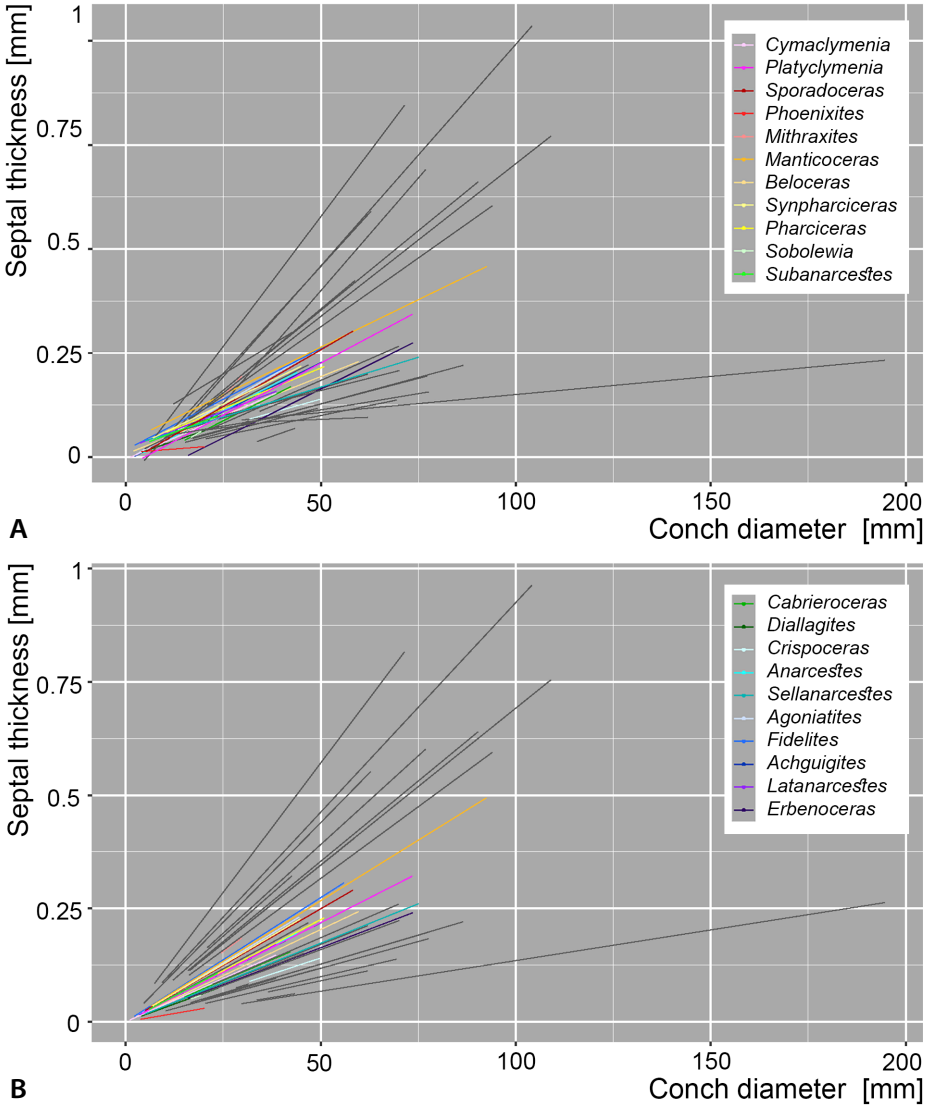


**Figure 8.** Linear biplot of the same data as in Figure 7 (same colour-coding of genera), with additional data from Weber *et al.* (2022) (grey lines). • A – linear regression lines with slope = septal slope factor. • B – linear regression lines with intercept = 0 and slope = adjusted septal slope factor.

**Table 3.** Correlation of all environmental factors analysed in this study with the adjusted septal slope factor (short: aSSF) and the septal slope factor (short: SSF) of each genus, as well as the Genus–Age–Midpoint (average of lower and upper boundary of each genus; ages after GTS2020 (Gradstein *et al.* 2020), lower and upper boundary from literature; see Material and methods, Correlation of timescales). The values of the abiotic factors represent the median of all data within the lower and upper boundary of the genus (see Material and methods, Correlation of timescales). Sources to palaeoenvironmental data are found in the first row.

| | this study | this study | Genus–Age–Midpoint [Ma] absolute ages after GTS2020 (Gradstein *et al.* 2020) | Brugger *et al.* (2019) | Brugger *et al.* (2019) | van Geldern (2004) | van Geldern (2004) | van Geldern (2004) | Brachiopods Grossman & Joachimski (2020) | Conodonts Grossman & Joachimski, (2020) | Joachimski *et al.* (2005) |
|---|---|---|---|---|---|---|---|---|---|---|---|
| Genus | aSSF | SSF | Age [Ma] | $pCO_2$ [ppm] | SST [°C] | $\delta^{13}C$ [‰] | $\delta^{18}O$ [‰] | $^{87}Sr/^{86}Sr$ | $\delta^{18}O$ [‰] | $\delta^{18}O$ [‰] | $\delta^{11}B$ [‰] |
| *Cymaclymenia* | 0.0038 | 0.0041 | 361.05 | 699.76 | 26.97 | no data | no data | no data | −5.64 | 17.93 | no data |
| *Platyclymenia* | 0.0044 | 0.0050 | 363.40 | 813.17 | 28.81 | no data | no data | no data | −5.98 | 17.64 | no data |
| *Sporadoceras* | 0.0050 | 0.0054 | 363.80 | 830.05 | 27.85 | no data | no data | no data | −6.00 | 17.58 | no data |
| *Phoenixites* | 0.0015 | 0.0007 | 370.35 | 969.99 | 29.77 | 2.81 | −4.98 | 0.7080655 | −5.00 | 17.73 | no data |
| *Manticoceras* | 0.0053 | 0.0046 | 374.30 | 1271.95 | 28.33 | 0.04 | −5.54 | 0.7080280 | −5.68 | 19.67 | 6.70 |
| *Beloceras* | 0.0041 | 0.0037 | 373.80 | 1334.94 | 28.33 | 0.04 | −5.54 | 0.7080280 | −5.68 | 19.60 | 6.70 |
| *Synpharc.* | 0.0051 | 0.0045 | 379.35 | 1298.33 | 22.06 | 0.86 | −5.13 | 0.7078740 | −4.55 | 18.99 | 7.30 |
| *Pharciceras* | 0.0045 | 0.0039 | 379.90 | 1243.37 | 24.61 | 0.89 | −5.30 | 0.7078660 | −4.59 | 18.95 | 7.30 |
| *Agoniatites* | 0.0052 | 0.0054 | 387.40 | 1061.78 | 22.46 | 2.21 | −3.00 | 0.7078265 | −2.89 | 18.36 | 12.20 |
| *Cabrieroc.* | 0.0037 | 0.0047 | 387.65 | 1061.78 | 20.58 | 1.35 | −2.95 | 0.7078510 | −2.88 | 18.39 | 12.20 |
| *Diallagites* | 0.0031 | 0.0032 | 389.80 | 1191.59 | 22.46 | 1.39 | −2.92 | 0.7078495 | −2.84 | 18.62 | 13.55 |
| *Sobolewia* | 0.0030 | 0.0055 | 385.60 | 1055.41 | 22.68 | 2.10 | −3.12 | 0.7078255 | −2.93 | 18.33 | 11.15 |
| *Subanarcestes* | 0.0046 | 0.0035 | 389.50 | 1152.55 | 22.33 | 1.38 | −2.91 | 0.7078535 | −2.84 | 18.59 | 13.55 |
| *Fidelites* | 0.0055 | 0.0049 | 389.45 | 1191.59 | 22.06 | 1.37 | −2.91 | 0.7078480 | −2.84 | 18.58 | 13.10 |
| *Mithraxites* | 0.0062 | 0.0102 | 388.95 | 1113.50 | 22.33 | 1.38 | −2.91 | 0.7078495 | −2.85 | 18.54 | 13.10 |
| *Crispoceras* | 0.0028 | 0.0026 | 390.00 | 1244.22 | 22.52 | 1.39 | −2.92 | 0.7078495 | −2.84 | 18.64 | 13.55 |
| *Anarcestes* | 0.0045 | 0.0049 | 394.60 | 1780.37 | 22.06 | 0.96 | −2.86 | 0.7078780 | −2.87 | 18.44 | 12.60 |
| *Achguigites* | 0.0044 | 0.0047 | 397.40 | 1780.95 | 20.27 | 0.71 | −3.35 | 0.7079190 | −3.07 | 18.10 | 12.95 |
| *Sellanarcestes* | 0.0035 | 0.0029 | 397.70 | 1775.45 | 19.70 | 0.63 | −3.41 | 0.7079330 | −3.09 | 18.07 | 12.95 |
| *Latanarcestes* | 0.0044 | 0.0036 | 396.80 | 1797.94 | 21.41 | 0.89 | −2.87 | 0.7079055 | −3.02 | 18.16 | 12.95 |
| *Erbenoceras* | 0.0033 | 0.0047 | 403.60 | 1761.39 | 29.53 | 1.20 | −3.17 | 0.7080410 | −3.40 | 17.44 | 13.90 |

environmental data is determined, vary from study to study. The data for the atmospheric $CO_2$ (Brugger *et al.* 2019) is originally from Foster *et al.* (2017) and uses absolute ages from Gradstein (2012). The proxy data for the isotopic sea surface temperature (Brugger *et al.* 2019) is from Joachimski *et al.* (2009) and use the absolute ages from Gradstein & Ogg (2004). All the data from van Geldern (2004: $\delta^{13}C$, $\delta^{18}O$, $^{87}Sr/^{86}Sr$) has been updated to Menning & Hendrich (2002). The $\delta^{18}O$-values of brachiopods and conodonts were obtained from Grossman & Joachimski (2020) who employed the GTS2020 timescale (Becker *et al.* 2020). Joachimski *et al.* (2005) do not provide a reference timescale for the absolute ages of the $\delta^{11}B$. The data includes the stage for each datapoint, but this does not provide enough information for a correct mapping, and therefore the absolute age-values for the $\delta^{11}B$ are taken directly from Joachimski *et al.* (2005). Fortunately, the best fit of all available timescales for the age values of Joachimski *et al.* (2005) is the GTS2020 and only a negligible number of datapoints have shifted slightly since its publication. To analyse the environmental data with respect to the septal thickness,

**Table 4.** Results of Mann-Kendall and Shapiro-Wilk tests with *p*-values adjusted for multiple comparisons using false discovery rate (FDR). The abiotic data is from Brugger *et al.* (2019) for $pCO_2$ and SST°C, van Geldern 2004 for $\delta^{13}C_{brachiopods}$ and $\delta^{18}O_{brachiopods,}$ Grossman & Joachimski (2020) for $\delta^{18}O_{brachiopods}$ and $\delta^{18}O_{conodonts}$, and Joachimski *et al.* (2005) for $\delta^{11}B_{brachiopods}$.

| | Mann-Kendall | | | Shapiro-Wilk | | |
|---|---|---|---|---|---|---|
| | τ | 2-sided p | p (FDR) | W | p | p (FDR) |
| aSSF | −0.0762 | 0.6506 | 0.8132 | 0.9750 | 0.8397 | 0.8397 |
| SSF | −0.0476 | 0.7858 | 0.8731 | 0.8362 | 0.0025 | 0.0031 |
| $pCO_2$ | 0.6530 | 2.22E−16 | 7.40E−16 | 0.9442 | 7.17E−05 | 0.0001 |
| SST°C | −0.0022 | 0.9344 | 0.9344 | 0.9781 | 3.357E−08 | 6.71E−08 |
| $\delta^{13}C_{brachiopods}$ | 0.1220 | 3.27E−04 | 8.18E−04 | 0.9748 | 2.56E−06 | 4.26E−06 |
| $\delta^{18}O_{brachiopods}$ | 0.4730 | 2.22E−16 | 7.40E−16 | 0.9463 | 9.992E−11 | 3.33E−10 |
| $^{87}Sr/^{86}Sr_{brachiopods}$ | −0.2040 | 0.0115 | 0.0191 | 0.7490 | 9.149E−10 | 2.29E−09 |
| $\delta^{18}O_{brachiopods}$ | −0.0842 | 5.69E−04 | 0.0011 | 0.9229 | 2.2E−16 | 1.10E−15 |
| $\delta^{18}O_{conodonts}$ | −0.4460 | 2.22E−16 | 7.40E−16 | 0.9383 | 2.2E−16 | 1.10E−15 |
| $\delta^{11}B_{brachiopods}$ | 0.2520 | 0.1733 | 0.2476 | 0.9593 | 0.6175 | 0.6861 |

the absolute ages of the abiotic factors and the temporal occurrence of the ammonoid genera used in this study were correlated. First, ammonoid and conodont zones of the included ammonoid materials were extracted from the literature (Becker & House 1994; Belka *et al.* 1999; Korn 1999; Korn *et al.* 2000; Klug 2001, 2002; Monnet *et al.* 2011; Korn & Klug 2015), and the obtained stratigraphic data were correlated with the absolute age provided in the GTS2020 (Becker *et al.* 2020). Therewith, the lower and upper boundaries of the temporal occurrence of the ammonoid genera were determined (Fig. 9). The age-midpoint of each genus was calculated by taking the mean age of those lower and upper boundaries. To compare the influence of the environmental factors on the septal thickness, the differing timescales were harmonized, and the age of the environmental factors was transformed to fit the GTS2020. Since the only invariable time indications are the stage boundaries, the ages of the old timescales were mapped within the different stages (Fig. 10). To test whether the septal thickness correlates with the environmental factors, the median of all datapoints within the temporal occurrence (between the lower and upper boundary) of each genus was calculated. In case of gaps in the environmental data, the first datapoint below the lower boundary and the first datapoint above the upper boundary were taken to calculate the mean of the two points. This results in one value from each abiotic factor for each genus (Tab. 3).

## Phylogeny

To compare the septal thickness between different taxonomic groups and thus test the relationship between phylogeny and septal thickness, the adjusted septal slope factor of all genera belonging to the same suborder was averaged (Tab. 7). As far as the suborders Cyrtoclymeniina and Clymeniina are concerned, they

**Table 5.** Results of Fligner-Killeen test with *p*-values adjusted for multiple comparisons using false discovery rate (FDR).

| | Fligner-Killeen | | | | |
|---|---|---|---|---|---|
| | $\chi^2$ | critical $\chi^2$ | df | *p* | *p* (FDR) |
| aSSF ~ age | – | 31.410 | 20 | – | – |
| aSSF ~ $pCO_2$ | 19.708 | 28.869 | 18 | 0.350 | 0.764 |
| aSSF ~ SST°C | 19.047 | 24.996 | 15 | 0.212 | 0.764 |
| aSSF ~ $\delta^{13}C$ (v.G.) | 16.972 | 23.685 | 14 | 0.258 | 0.764 |
| aSSF ~ $\delta^{18}O$ (v.G.) | 11.911 | 22.362 | 13 | 0.535 | 0.764 |
| aSSF ~ $^{87}Sr/^{86}Sr$ | 12.194 | 23.685 | 14 | 0.591 | 0.764 |
| aSSF ~ $\delta^{18}O$ (Bra.) | 19.000 | 26.296 | 16 | 0.269 | 0.764 |
| aSSF ~ $\delta^{18}O$ (Con.) | – | 31.410 | 20 | – | – |
| aSSF ~ $\delta^{11B}$ | 6.476 | 15.507 | 8 | 0.594 | 0.764 |
| SSF ~ age | – | 31.410 | 20 | – | – |
| SSF ~ $pCO_2$ | 19.765 | 28.869 | 18 | 0.346 | 0.623 |
| SSF ~ SST°C | 19.025 | 24.996 | 15 | 0.213 | 0.623 |
| SSF ~ $\delta^{13}C$ (v.G.) | 16.742 | 23.685 | 14 | 0.270 | 0.623 |
| SSF ~ $\delta^{18}O$ (v.G.) | 11.903 | 22.362 | 13 | 0.536 | 0.803 |
| SSF ~ $^{87}Sr/^{86}Sr$ | 11.715 | 23.685 | 14 | 0.629 | 0.809 |
| SSF ~ $\delta^{18}O$ (Bra.) | 17.730 | 26.296 | 16 | 0.340 | 0.623 |
| SSF ~ $\delta^{18}O$ (Con.) | – | 31.410 | 20 | – | – |
| SSF ~ $\delta^{11B}$ | 11.487 | 15.507 | 8 | 0.176 | 0.623 |
| Age ~ $pCO_2$ | 20.000 | 28.869 | 18 | 0.333 | 0.675 |
| Age ~ SST°C | 14.512 | 24.996 | 15 | 0.487 | 0.675 |
| Age ~ $\delta^{13}C$ (v.G.) | 16.766 | 23.685 | 14 | 0.269 | 0.675 |
| Age ~ $\delta^{18}O$ (v.G.) | 12.282 | 22.362 | 13 | 0.505 | 0.675 |
| Age ~ $^{87}Sr/^{86}Sr$ | 12.194 | 23.685 | 14 | 0.591 | 0.675 |
| Age ~ $\delta^{18}O$ (Bra.) | 17.932 | 23.685 | 16 | 0.328 | 0.675 |
| Age ~ $\delta^{18}O$ (Con.) | – | 26.296 | 20 | – | – |
| SSF ~ $\delta^{11B}$ | 7.195 | 15.507 | 8 | 0.516 | 0.675 |

| | Spearman's rank correlation ρ correlation of abiotic factor with: | | | | | |
|---|---|---|---|---|---|---|
| | aSSF | | | SSF | | |
| abiotic factor | ρ | *p*-value | *p* (FDR) | ρ | *p*-value | *p* (FDR) |
| $pCO_2$ | 0.2917 | 0.2114 | 0.4228 | −0.0331 | 0.8913 | 0.9670 |
| SST°C | 0.0602 | 0.8016 | 0.9161 | 0.0105 | 0.9670 | 0.9670 |
| $\delta^{13}C_{brachiopods}$ | −0.2083 | 0.4208 | 0.6733 | 0.1078 | 0.6803 | 0.9670 |
| $\delta^{18}O_{brachiopods}$ | −0.3235 | 0.2050 | 0.4228 | −0.0392 | 0.8835 | 0.9670 |
| $^{87}Sr/^{86}Sr_{brachiopods}$ | −0.0809 | 0.7584 | 0.9161 | −0.3873 | 0.1255 | 0.9670 |
| $\delta^{18}O_{brachiopods}$ | −0.3068 | 0.1879 | 0.4228 | −0.0271 | 0.9114 | 0.9670 |
| $\delta^{18}O_{conodonts}$ | 0.3128 | 0.1791 | 0.4228 | −0.1429 | 0.5465 | 0.9670 |
| $\delta^{11}B_{brachiopods}$ | 0.0147 | 0.9607 | 0.9607 | −0.2000 | 0.4564 | 0.9670 |

**Table 6.** Results of Spearman's rank correlation test with *p*-values adjusted for multiple comparisons using false discovery rate (FDR). The abiotic data is from Brugger *et al.* (2019) for $pCO_2$ and SST°C, van Geldern (2004) for $\delta^{13}C_{brachiopods}$ and $\delta^{18}O_{brachiopods}$, Grossman & Joachimski (2020) for $\delta^{18}O_{brachiopods}$ and $\delta^{18}O_{conodonts}$, and Joachimski *et al.* (2005) for $\delta^{11}B_{brachiopods}$.

were grouped together as the order Clymeniida, because each of the two suborders are only represented by one genus each in this study. The phylogeny of the Devonian ammonoid taxa is based on the studies of Korn (2001) as well as Korn & Klug (2002) and is displayed in Figure 9. As a result, the 21 genera are grouped into five suborders (Agoniatitina: 5 genera, Anarcestina: 7, Pharciceratina: 2, Gephuroceratina: 2, Tornoceratina: 3) and one order (Clymeniida: 2). To test whether the variation of septal thickness is higher within or between phylogenetic lineages, the adjusted septal slope factor was plotted in a violin plot according to the taxonomic groups (Fig. 11A). Additionally, the septal thickness was plotted against the conch diameter, displaying the linear regression of all genera within each taxonomic group (Fig. 12). Furthermore, the ammonoid genera were categorized according to the Devonian stages. For the analyses, two of the stages were further subdivided, grouping the genera into seven-time bins (early Emsian, late Emsian, Eifelian, Givetian, Frasnian, early Famennian, late Famennian) (Tab. 8). Again, the data was visualized in a violin plot (Fig. 11B) and by plotting the linear regression for each stage (Fig. 13).

## Palaeogeography

The correlation between adjusted septal slope factor and palaeolatitude could not be examined in this study since all specimens are from the Anti-Atlas of Morocco and do have a similar palaeolatitude of approximately 40° south (Fig. 14A). However, the data was combined with the data of Mesozoic ammonoids from Weber *et al.* (2022) and the linear regressions of the aSSF for each genus (this study) and species (Weber *et al.* 2022) were plotted in Fig. 14B and coloured according to their absolute value of palaeogeographic latitude (northern and southern latitudes fused). For consistency, we followed the approach of Weber *et al.* (2022) using the data of Scotese (2001).

# Results

The measurements of septal thickness are provided in the supplementary table. To analyse the influence of environmental factors and phylogenetic relationships on the septal thickness, the SSF and the aSSF were calculated with linear regression models for each genus and averaged for each taxonomic group and time bin (Tabs 2, 7, 8). Both factors were used for statistical analysis and to visualize differences between and within taxonomic groups.

## Environmental parameters

All environmental factors used in this study and their data sources are listed in Table 3 together with their median value for each genus. They are displayed together with the adjusted septal slope factor over time in Figure 15. It should be noted that only $pCO_2$ and $\delta^{11}B$ are directly linked to seawater pH; all other parameters have primarily different drivers (biological pump, temperature,

**Figure 9.** Phylogenetic relationships of the 21 ammonoid genera examines in this study. Timescale from GTS2020 (Gradstein *et al.* 2020); Phylogeny after (Korn 2001, Korn & Klug 2002); grey bands represent extinction events (Choteč, Kačák, Kellwasser and Hangenberg); coloured rectangles show lower an upper boundary of the ammonoid genera (from literature; see previous section in Material and methods, Correlation of timescales); dotted lines only reflect qualitative phylogenetic relationship.

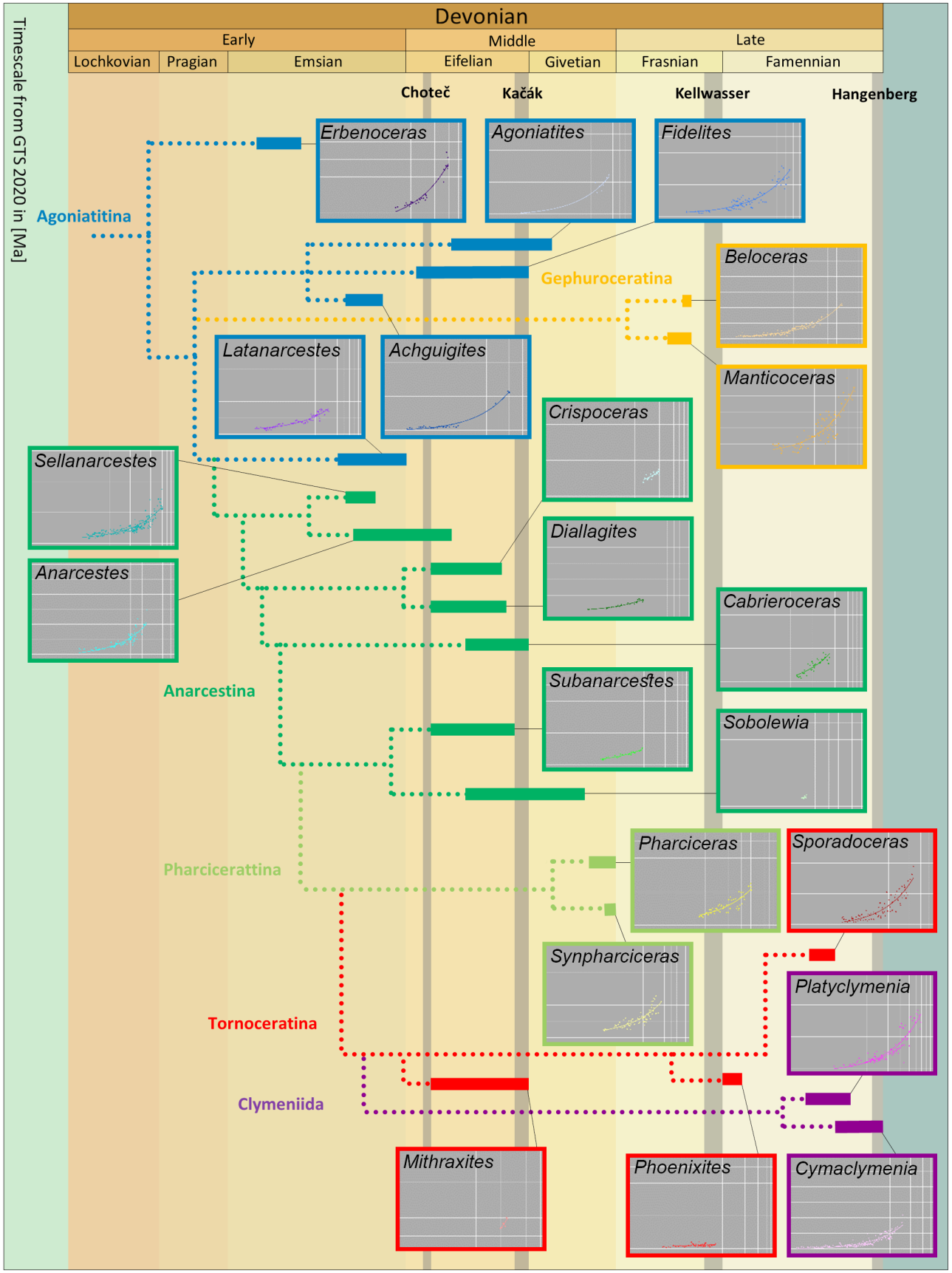
Timescale from GTS 2020 in [Ma]
Devonian
Early
Middle
Late
Lochkovian
Pragian
Emsian
Eifelian
Givetian
Frasnian
Famennian
Choteč
Kačák
Kellwasser
Hangenberg
Erbenoceras
Agoniatites
Fidelites
Agoniatitina
Gephuroceratina
Beloceras
Latanarcestes
Achguigites
Manticoceras
Crispoceras
Sellanarcestes
Diallagites
Anarcestes
Cabrieroceras
Anarcestina
Subanarcestes
Sobolewia
Pharciceras
Sporadoceras
Pharcicerattina
Synpharciceras
Platyclymenia
Tornoceratina
Clymeniida
Mithraxites
Phoenixites
Cymaclymenia

$$P_{new} = LSB_{new} - \frac{LSB_{old} - P_{old}}{LSB_{old} - USB_{old}}(LSB_{new} - USB_{new})$$

$P_{old}$ = Age Point on old Timescale

$P_{new}$ = Age Point on new Timescale

$LSB_{old}$ = Lower Stage Boundary on old Timescale

$LSB_{new}$ = Lower Stage Boundary new Timescale

$USB_{old}$ = Upper Stage Boundary on old Timescale

$USB_{new}$ = Upper Stage Boundary new Timescale

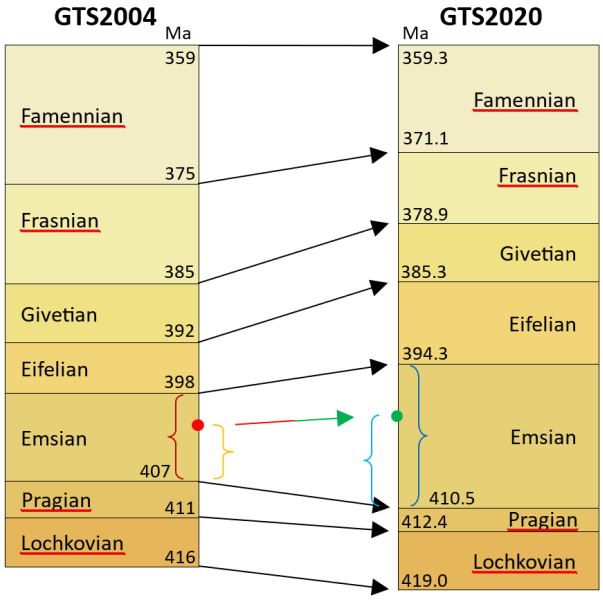


**Figure 10.** Correlation between an old (GTS2004) and a newer (GTS2020) timescale, showing the linear mapping within stages of an age point from the old to the new timescale. Colour-coding of stages after (Gradstein *et al.* 2020).

| Taxonomic Group | #genera | #specimen | mean | min | max | sd |
|---|---|---|---|---|---|---|
| Agoniatitina | 5 | 11 | 0.0046 | 0.0033 | 0.0055 | 0.0009 |
| Anarcestina | 7 | 19 | 0.0036 | 0.0028 | 0.0046 | 0.0007 |
| Pharcicerattina | 2 | 13 | 0.0048 | 0.0045 | 0.0051 | 0.0004 |
| Gephuroceratina | 2 | 8 | 0.0047 | 0.0041 | 0.0053 | 0.0009 |
| Tornoceratina | 3 | 8 | 0.0042 | 0.0015 | 0.0062 | 0.0025 |
| Clymeniida | 2 | 6 | 0.0041 | 0.0038 | 0.0044 | 0.0004 |

**Table 7.** Genera grouped according to suborder (exept for *Cymaclymenia* & *Platyclymenia* being grouped together in the order Clymeniida); (from left to right) taxonomic group, number of genera within each group, number of specimens within each group, mean aSSF, lowest aSSF, highest aSSF, standard deviation (sd). Visualization in Figures 11A, 12.

| Time Bin | #genera | #specimen | mean | min | max | sd |
|---|---|---|---|---|---|---|
| early Emsian | 1 | 2 | 0.0033 | 0.0033 | 0.0033 | – |
| late Emsian | 4 | 14 | 0.0042 | 0.0035 | 0.0045 | 0.0005 |
| Eifelian | 8 | 15 | 0.0043 | 0.0028 | 0.0062 | 0.0013 |
| Givetian | 2 | 13 | 0.0048 | 0.0045 | 0.0051 | 0.0004 |
| Frasnian | 2 | 8 | 0.0047 | 0.0041 | 0.0053 | 0.0009 |
| early Famennian | 1 | 4 | 0.0015 | 0.0015 | 0.0015 | – |
| late Famennian | 3 | 9 | 0.0044 | 0.0038 | 0.0050 | 0.0006 |

**Table 8.** Genera grouped according to their time bin (from left to right) time bin, number of genera within each group, number of specimens within each group, mean aSSF, lowest aSSF, highest aSSF, standard deviation (sd). Visualization in Figures 11B, 13.

continental weathering) but might reflect changing seawater pH indirectly.

The generalized differencing of time model including the Spearman correlation coefficient shows neither a correlation between the septal slope factor and any of the abiotic factors, nor between the adjusted septal slope factor and the abiotic factors. All correlation coefficients ρ are close to 0, indicating no monotonic trend being present, however they are not statistically significant since their *p*-values are above the critical value of 0.05 (Tab. 6, Fig. 16).

## Phylogeny

The SSF and aSSF of each genus is listed in Table 5 and visualized in Figures 7 and 8. The aSSF was summarized for each taxonomic group (Tab. 7) and time bin (Tab. 8) and the variation within and between these groups was visualized in Figures 11 (violin plots), 12 and 13 (biplots). In Figure 8A, the difference between the SSF and the aSSF (Fig. 8B) is apparent. The adjusted septal slope factor is more reliable in reflecting the true septal thickness, than the septal slope factor introduced by Weber *et al.* (2022).

Genera with a linear regression line in the lower part of the biplot have thinner septa, which is reflected in a small adjusted septal slope factor, while genera with regression lines in the upper part of the biplot have thicker septa, which is reflected in a greater adjusted septal slope factor, respectively. This trend does not necessarily hold true in the septal slope factor, especially when the error of measurement is high, or the genus has only a low number of measurable septa close together. The deviation of the SSF from the true septal thickness is also amplified in

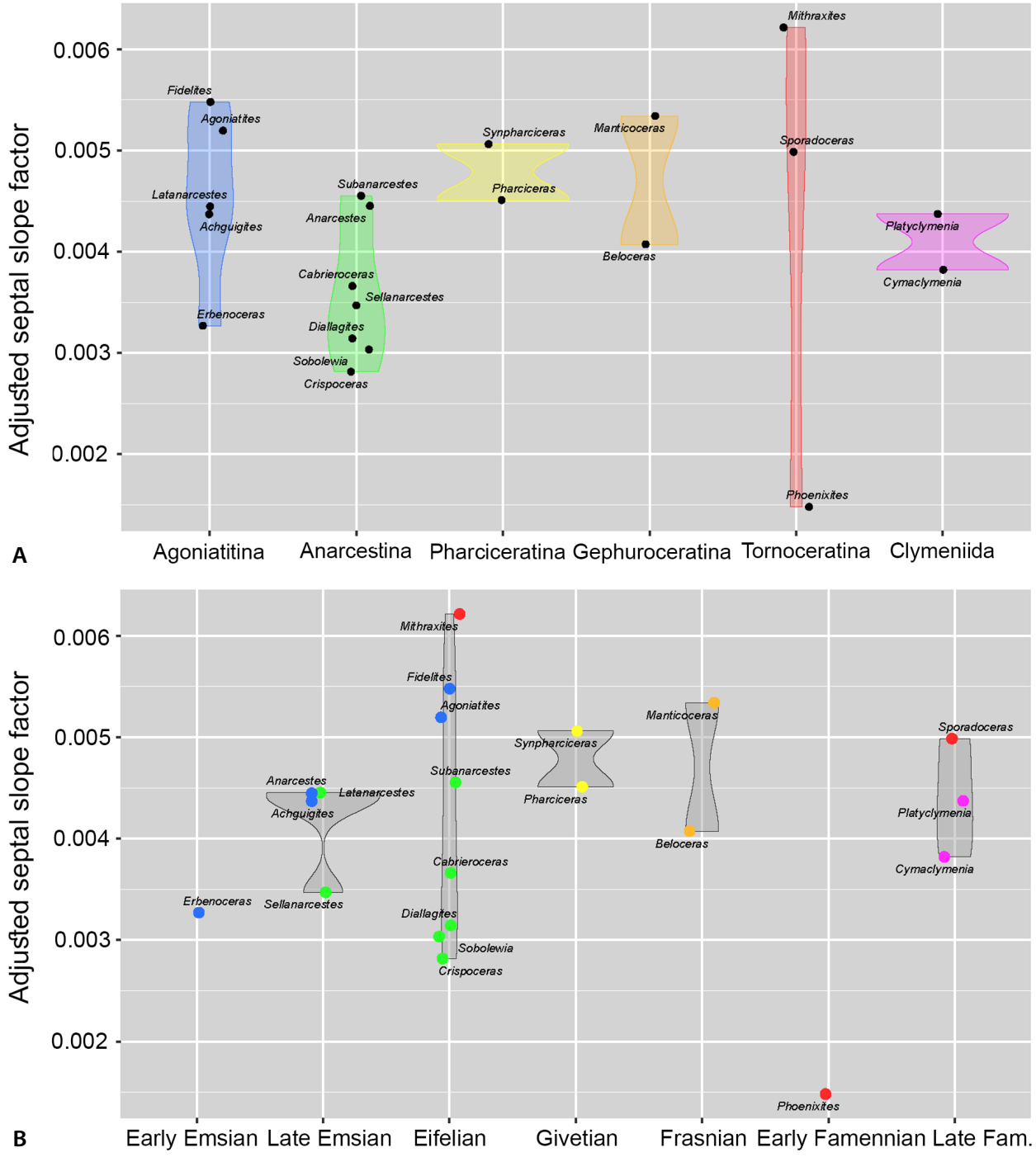


**Figure 11.** Violin plots of: A – adjusted septal slope factor grouped by taxonomy: five suborders (Agoniatitina, Anarcestina, Pharcicerattina, Gephuroceratina, Tornoceratina) and one order (Clymeniida); and • B – adjusted septal slope factor grouped by time bins: early Emsian, late Emsian, Eifelian, Givetian, Frasnian, early Famennian, late Famennian.

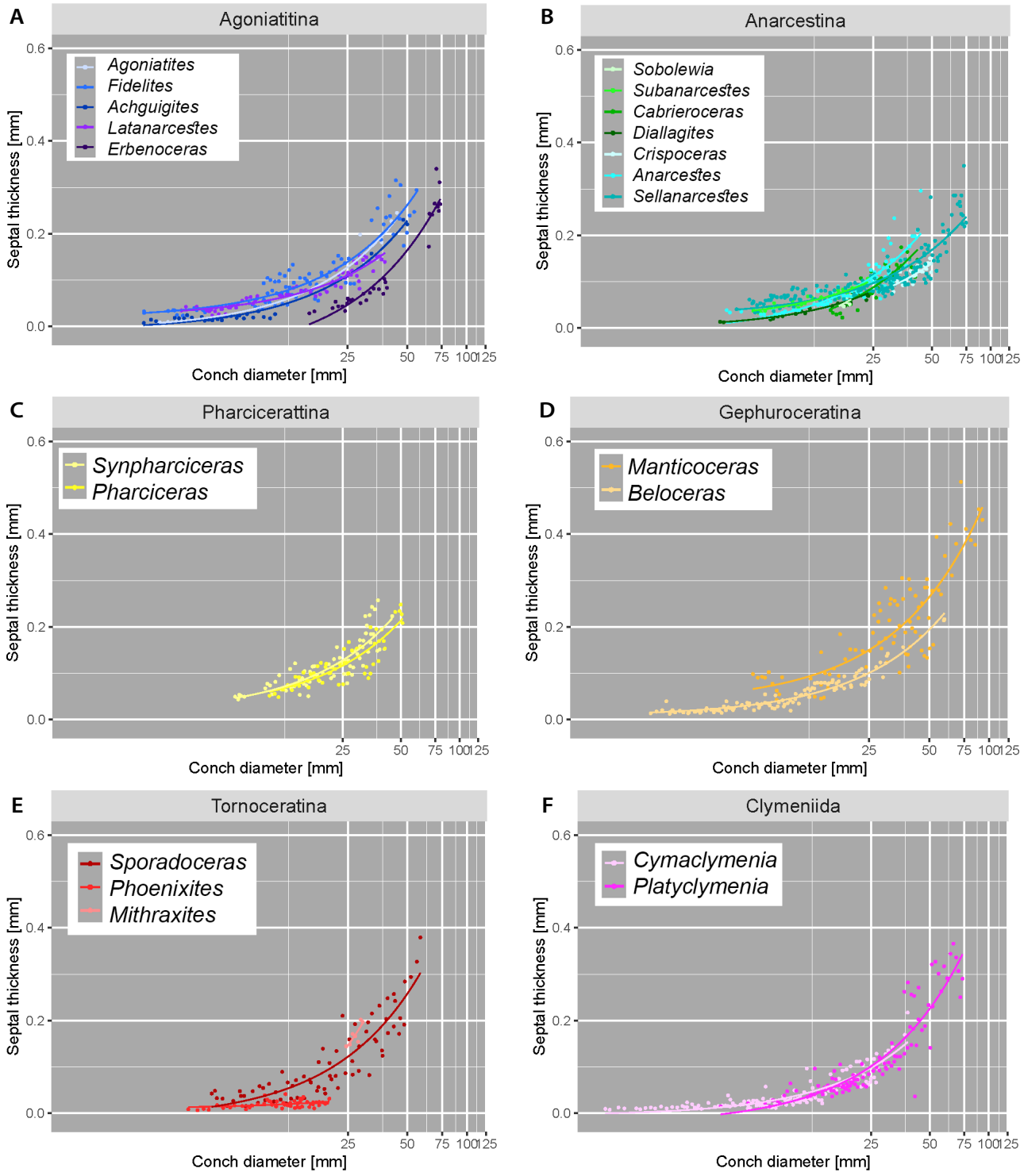


**Figure 12.** Semilogarithmic biplots of septal thickness versus conch diameter (same data as Fig. 7). Genera grouped by suborder.

smaller specimens and less visible in larger ones, as was the case in the study of Weber *et al.* (2022; Fig. 8 herein).

There is weak evidence for a monotonic trend of the aSSF throughout the Devonian (Mann-Kendall test; *p*-value = 0.65; Tab. 4). In the early Emsian, directly after the origin of ammonoids, the adjusted septal slope factor starts out low with *Erbenoceras* (0.0033) within the suborder Agoniatitina and reaches its average value of 0.0042 during the late Emsian (Fig 15A). After the Choteč Event in the early Eifelian up to the Kačák Event at the

**Table 9.** Comparison of aSSF, SSF and Intercept between Devonian ammonoids (this study) and Mesozoic ammonoids (Weber *et al.* 2022). Mean value (mean), lowest value (min), highest value (max), standard deviation (sd). Visualization in Figure 8.

| | mean | min | max | sd |
|---|---|---|---|---|
| aSSF (this study) | 0.0042 | 0.0015 | 0.0062 | 0.0011 |
| aSSF (Weber et al. 2020) | 0.0046 | 0.0014 | 0.0114 | 0.0029 |
| SSF (this study) | 0.0044 | 0.0007 | 0.0102 | 0.0017 |
| SSF (Weber et al. 2020) | 0.0048 | 0.0004 | 0.0124 | 0.0035 |
| Intercept (this study) | −0.0074 | −0.1091 | 0.0359 | 0.0343 |
| Intercept (Weber et al. 2020) | −0.0093 | −0.1414 | 0.0699 | 0.0508 |

Eifelian–Givetian boundary, the aSSF shows extremely high variation (0.0028 to 0.0062). During this time, genera within the suborder Anarcestina are on the lower end (mean value of 0.0034), while *Agoniatites* (0.0052) and *Fidelites* (0.0055) of the suborder Agoniatitina show a higher adjusted septal slope factor. The overall highest aSSF is found in the Eifelian within the suborder Tornoceratina and belongs to *Mithraxites* (0.0062). In the Givetian, we only have representatives of the Pharciceratitina and in the Frasnian, the only genera used in this study are from the suborder Gephuroceratina. Therefore, it is uncertain whether the diversity in the adjusted septal slope factors and the septal thickness declined during this time or was biased by the small sample size.

The lowest adjusted septal slope factor by far is found within the suborder Tornoceratina and belongs to *Phoenixites* (0.0015) from the early Famennian, right after the Kellwasser Event, one of the big five mass extinction events (Carmichael *et al.* 2014). In the late Famennian, *Sporadoceras*, also from the suborder Tornoceratina, shows a comparatively high adjusted septal slope factor of 0.0050. The two representatives of the order Clymeniida stand with an average to low adjusted septal slope factor at the end of the Famennian. Overall, there appears to be a high correlation between aSSF and taxonomic relationship (Fig. 11A). A noticeable exception is found in the suborder Tornoceratina with the greatest aSSF (*Mithraxites*) in the Eifelian (0.0062), the lowest aSSF (*Phoenixites*) in the early Famennian (0.0015), and again a high aSSF (*Sporadoceras*) in the late Famennian (0.0050) (Fig. 12E). When comparing the adjusted septal slope factor of the Devonian ammonoids with the data of Mesozoic ammonoids from Weber *et al.* (2022), it becomes apparent that the variation of septal thickness in Mesozoic ammonoids is significantly higher (Tab. 9, Fig. 8).

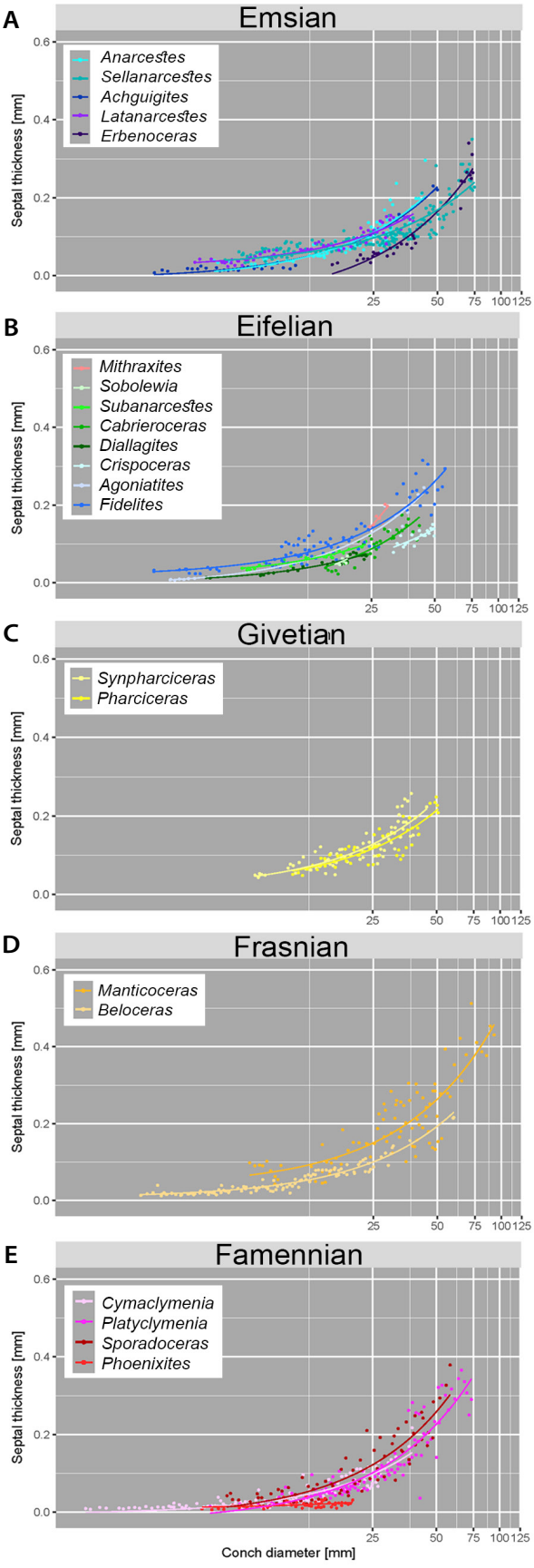


**Figure 13.** Semilogarithmic biplots of septal thickness versus conch diameter (same data as Fig. 7). Genera grouped by stages: A – Emsian; B – Eifelian; C – Givetian; D – Frasnian; E – Famennian.

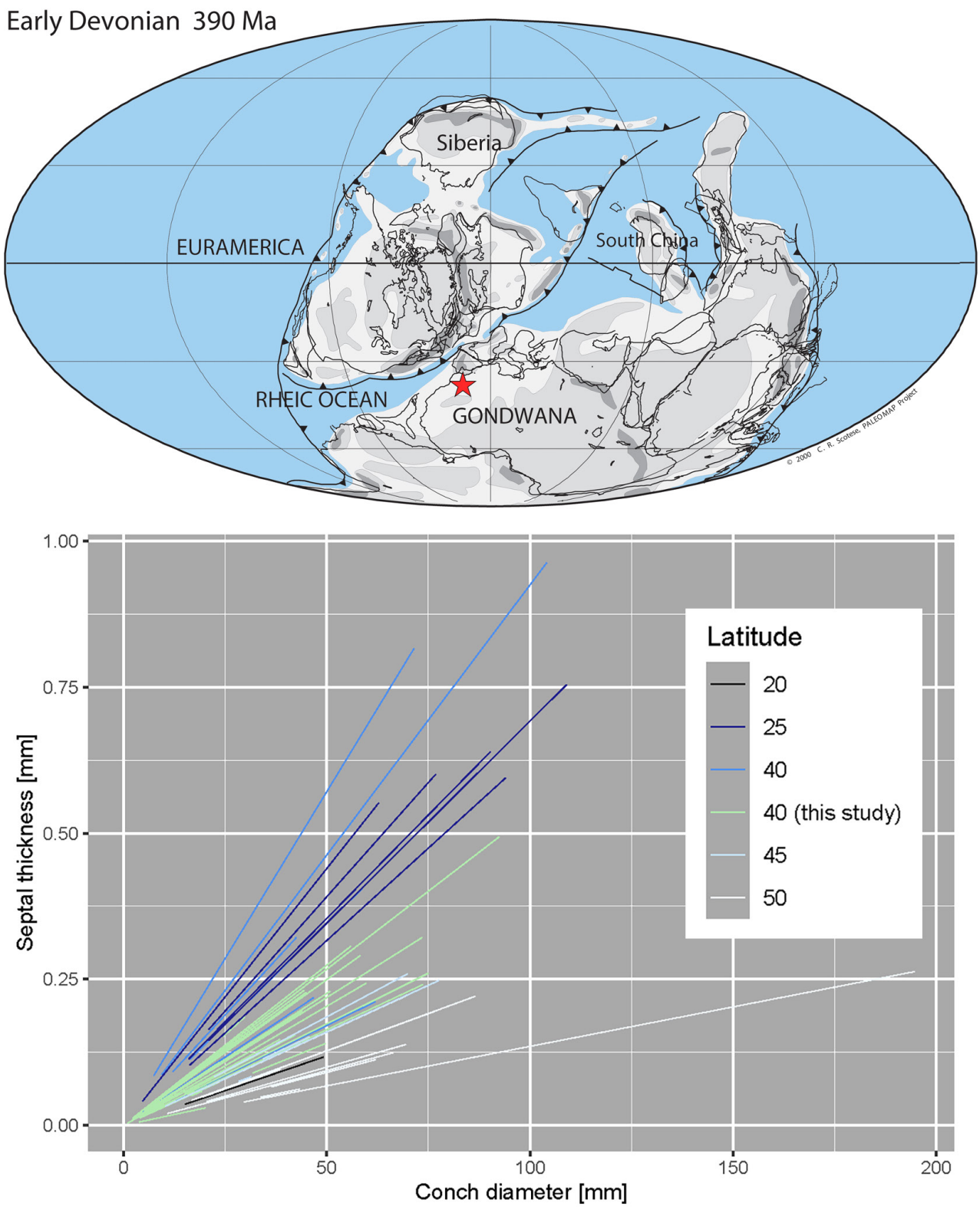


**Figure 14.** Top – palaeogeographic reconstruction for the Early Devonian (Scotese 2001) and origin of the specimens examined in this study (red star: Anti-Atlas of Morocco, latitude: approximately 40° south). Bottom – linear biplot (same as in Fig. 8B) with data from this study (green) and (Weber *et al.* 2022) (blue); lines represent linear regression lines with intercept = 0 and slope = adjusted septal slope factor for each genus; colours represent absolute value of palaeogeographic latitude (northern and southern latitudes fused).

### Palaeogeography

The adjusted septal slope factors for each genus (this study) and species (Weber *et al.* 2022) were plotted in Figure 14A and coloured according to their absolute value of palaeogeographic latitude (northern and southern latitudes fused). The Devonian ammonoids examined in this study all have their origin in the Anti-Atlas of Morocco with a palaeolatitude of approximately 40° south. The range of aSSF of these Devonian ammonoids fit well with the data of Mesozoic ammonoids by Weber *et al.* (2022). It should be noted that paleolatitude data can differ markedly throughout the Devonian depending on the reconstruction (for a recent one see Torsvik *et al.* 2025).

## Discussion

### Palaeoenvironment

Weber *et al.* (2022) hypothesize that in times of decreased seawater saturation with respect to $CaCO_3$ and thus a reduction of seawater pH, there is a positive selection for ammonoids with thinner septa. Under these conditions, the deposition of aragonite and high-Mg calcite, and to a lesser extend low-Mg calcite is supressed, which may put biocalcifying organisms with aragonitic or high-Mg calcitic skeletons in a competitive disadvantage. This would probably contribute to a higher chance of survival of organisms that need less carbonate for their skeletons such as ammonoids with thinner septa (Hautmann 2004, Cohen & Holcomb 2009, Weber *et al.* 2022). Weber *et al.* (2022) therefore suggested a decrease in septal slope factor following a strong decline in oceanic pH-levels. To test if this is the case in Devonian ammonoids, the adjusted septal slope factor of the genera was compared with oceanic pH. Since we do not have estimates for sea surface pH for the Devonian in sufficient resolution, we correlated the adjusted septal slope factor with various proxy data.

One possible method for determining ocean water pH is boron isotopes ($\delta^{11}B$), although its reliability has been questioned (*e.g.* Joachimski *et al.* 2005, Hönisch *et al.* 2012). Some studies have suggested a correlation between the pH of seawater and $\delta^{11}B$ of marine biogenic carbon (Penman *et al.* 2013, Rasbury & Hemming 2017). Joachimski *et al.* (2005) examined the $\delta^{11}B$ of brachiopods from the Silurian (Sweden), Devonian (Morocco, China, USA), Pennsylvanian (USA) and Early Permian (Oman) (higher pH – enrichment of $^{11}B$ in marine organisms, but see Jurikova *et al.* 2019). The $\delta^{11}B$ of brachiopods (Joachimski *et al.* 2005) show a rise during the Emsian, a decrease in the Middle Devonian and a slight increase again in the Frasnian, right before the Kellwasser Event in the late Frasnian (Fig. 15G). However, species-specific vital effects seem to play a significant role, therefore some studies suggest that the $\delta^{11}B$ of brachiopods cannot be used as a palaeo-proxy on longer timescales, until further data resolves these issues (Joachimski *et al.* 2005). Additionally, the somewhat low temporal resolution of the data does not allow for comparisons with our data.

The $\delta^{18}O$ of biogenic carbon provides information on water temperature (Joachimski *et al.* 2009, Grossman & Joachimski 2020). Although the $\delta^{18}O$ of biogenic carbon does not directly indicate the pH, the trends in sea surface temperatures are linked with global temperatures, which are connected to atmospheric $CO_2$ and thus also to sea surface pH (Ridgwell & Zeebe 2005, Kump *et al.* 2009). Joachimski *et al.* (2009) suggested that Devonian conodonts lived close to the sea surface and are therefore reliable for the reconstruction of sea surface temperatures. The $\delta^{18}O$ of conodonts (Joachimski *et al.* 2009) shows low values (~ 17.5‰) in the Early Devonian, followed by a steady increase during the Middle Devonian with relatively high values (~ 20.0‰) in the late Emsian to Givetian. The $\delta^{18}O$ value decreases in the Frasnian and shows relatively low values (~ 17.5‰) again in the late Frasnian to Famennian. Because higher sea water temperatures result in lower $\delta^{18}O$ in the apatite (van Geldern 2004), the temperature curve for the Devonian (Fig.15C) is the exact inverse of the $\delta^{18}O$-curve, with high temperatures in the Early Devonian, a steady decrease during the Middle Devonian with a cooler climate in the late Emsian to Givetian, a warming trend in the Frasnian and relatively high temperatures in the late Frasnian to Famennian. The positive excursion in $\delta^{18}O$ in the earliest Famennian was interpreted as a short-term cooling episode, resulting from an increased burial of organic carbon at the Kellwasser horizons and accompanied lowering of atmospheric $CO_2$ (Joachimski *et al.* 2009).

Brachiopods construct their shells using low-magnesium calcite (Simonet Roda *et al.* 2019), which, in contrast to high-magnesium calcite and aragonite, is stable during diagenesis (Collins *et al.* 1991). Thus, their stable isotope content is considered well-suited for providing information about the geochemical composition of past oceans (van Geldern 2004, van Geldern *et al.* 2006). Additionally, the secondary and tertiary layers of modern brachiopod shell are in isotopic equilibrium with the ocean water during mineralisation (van Geldern *et al.* 2006), although some suggested that the $\delta^{18}O$ of brachiopods is less reliable (Joachimski *et al.* 2009). The $\delta^{18}O$ trends of conodonts in the Devonian (Joachimski *et al.* 2009) are comparable with the $\delta^{18}O$ brachiopod calcite (van Geldern 2004, Grossman & Joachimski 2020). According to van Geldern (2004), the most important influences on

oxygen isotope composition of carbonates is the $\delta^{18}O$ of the ocean water ($\delta^{18}O_W$) and the pH and temperature of the ocean water during precipitation. Some studies suggest no significant change in $\delta^{18}O$ of ocean waters in earth's history (Land & Leo Lynch 1996, Muehlenbachs 1998), whereas some have shown that $\delta^{18}O$ did not stay constant throughout the past (Veizer *et al.* 1997, 1999) and needs to be accounted for in isotopic temperature estimations (van Geldern 2004). The ocean water pH does have an inverse effect on the $\delta^{18}O$ of brachiopod calcite (low pH increases the $\delta^{18}O$, van Geldern *et al.* 2006). During high temperatures, increased atmospheric $CO_2$ and low ocean water pH, the $\delta^{18}O$ of brachiopod calcite shows lower values than expected, which can lead to the underestimation of the sea surface temperature (van Geldern *et al.* 2006). The same effect is reflected in the carbon isotope concentration trends ($\delta^{13}C$), where a low sea water pH leads to a higher $\delta^{13}C$ of the brachiopod calcite (Bijma *et al.* 1999, van Geldern 2004). With the same dependency of $\delta^{13}C$ on sea water temperatures, it is not surprising that the carbon isotope curve shows similar trends than the oxygen isotope curve (Fig. 15D, E) (van Geldern *et al.* 2006). According to van Geldern (2004), positive $\delta^{13}C$ excursions correlate with an increased proportion of organic carbon at the Kačák Event and the Lower and Upper Kellwasser Events, while the oxygen isotope curve displays two positive $\delta^{18}O$ excursions at the Kellwasser Events as well, indicating a decrease in temperature, which is likely due to temporary declines in atmospheric $CO_2$. The $CO_2$ models (Fig. 15B) (Berner & Kothavala 2001, Foster *et al.* 2017, Brugger *et al.* 2019) agree with the trends of higher temperatures in the Early Devonian and a steady decreasing of $CO_2$ and temperature during the Middle Devonian, but they do not show a rise in $pCO_2$ during the Frasnian (Joachimski *et al.* 2009), which would be expected with the decline of isotopic oxygen and the implied rise in temperature. According to Joachimski *et al.* (2009), $CO_2$ proxy data from $\delta^{13}C$ content of soil carbonate are too sparse to reconstruct short term variations in atmospheric $CO_2$ during the Middle to Late Devonian. Further support for the rise in temperature during the Frasnian comes from spreading tropical floras into higher latitudes during the Frasnian (Streel *et al.* 2000, Joachimski *et al.* 2009). Miospores reached their maximum latitudinal distribution in the latest Frasnian consistent with warm to very warm climatic conditions during the Frasnian–Famennian transition (Streel *et al.* 2000, Joachimski *et al.* 2009).

Notably, the reconstructed temperature record in the Devonian has the same pattern as the $^{87}Sr/^{86}Sr$ from brachiopod calcite (Fig. 15F), with a continuous decrease in the Early Devonian, a low plateau in the Eifelian and early Givetian and an increase in the late Givetian with the highest values at the Devonian–Carboniferous boundary (van Geldern 2004, Joachimski *et al.* 2009). The increase in $^{87}Sr/^{86}Sr$ during the late Middle Devonian and Frasnian may result from intensified continental weathering, enhanced volcanic $CO_2$ release and climatic warming (van Geldern *et al.* 2006, Joachimski *et al.* 2009, Salifu *et al.* 2018). The increase in weathering may have its origins in the evolution of arborescence and seed habit in land plants (Berner *et al.* 1995, Algeo *et al.* 2001). The increase in size, geographical distribution, and root biomass of vascular plants may have contributed substantially to the increase in chemical weathering, causing a pulse in nutrient flux to the oceans, resulting in eutrophication and thus stimulating marine algal blooms (Berner *et al.* 1995). This caused widespread oceanic anoxia, leading to the various Devonian biotic crisis (Berner *et al.* 1995). Additionally, the increase in plant-biomass may have contributed to the decrease of atmospheric $CO_2$ and caused short term cooling events during the Middle and Late Devonian (Berner *et al.* 1995). Contrastingly, new evidence suggests volcanism as additional trigger for the global environmental perturbations that occurred during the late Frasnian (Rakocinski *et al.* 2023, Marshall *et al.* 2025). Volcanogenic $CO_2$ emissions could thus have caused short pulses of higher temperature and decreasing seawater pH, which could have affected marine biocalcifiers. The current evidence thus shows that during the late Frasnian, the environmental conditions were highly volatile including phases of high global temperatures.

## Kellwasser event and ocean acidification

The Kellwasser biotic crisis, one of the big five mass extinction events in Earth's history (McGhee *et al.* 2013), happened in the Late Devonian at the Frasnian–Famennian boundary (Carmichael *et al.* 2014, Becker *et al.* 2020). It is accompanied by short-term cycles of cooling and warming and is visible in the geologic record as geographically widely distributed black shale layers (Berner *et al.* 1995). These black shale layers were deposited during anoxic environments in the ocean, which were most likely driven by episodic eutrophication of sea surface waters (Berner *et al.* 1995, Carmichael *et al.* 2014, Barash 2016). Despite the rapid cooling episodes, which were caused by a decline in atmospheric $CO_2$ and made the sea surface pH rise (Ridgwell & Zeebe 2005, Clarkson *et al.* 2015, Ge *et al.* 2022), there is evidence for several anoxic events, which suggest phases of low pH and several temporary ocean acidification events during the deposition of the sediments of the lower and upper Kellwasser levels (Berner *et al.* 1995, Carmichael *et al.* 2014, Barash 2016). Based on the fossil record of biogenic reefs and marine organisms, Kiessling & Simpson (2011) noted that there

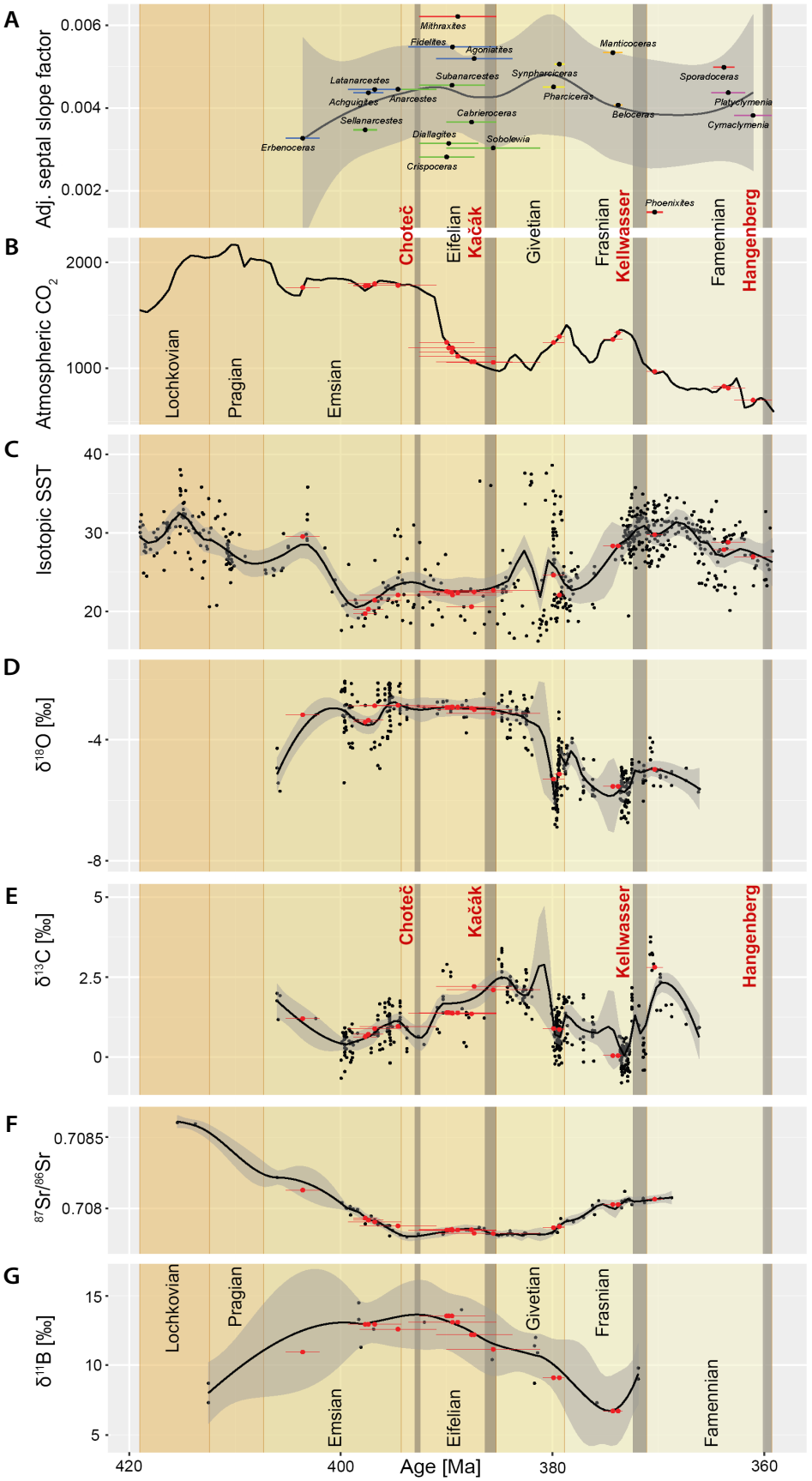


**Figure 15.** Correlation of adjusted septal slope factor and abiotic factors (vertical axis) over time (horizontal axis). Stages (Eifelian, Emsian, Givetian, Frasnian, Famennian) are shown in different background colours (Gradstein *et al.* 2020), grey bands represent extinction events (Choteč, Kačák, Kellwasser, Hangenberg). Red dots represent the average value of the abiotic factor for each genus at the Genus-Age-Midpoint, red lines show the lower and upper boundary of each genus (quantitative values and Age-Midpoints are found in Tab. 3); black lines show loess fit curves, grey bands indicate 95%-confidence-intervals. • A – adjusted septal slope factor of the 21 genera examined in this study. Black dots represent the specific adjusted septal slope factor at the Age-Midpoint of each genus; lines show the lower and upper boundary of each genus and are coloured according to the taxonomic group. • B – atmospheric $CO_2$ (Foster *et al.* 2017, Brugger *et al.* 2019). • C – isotopic sea surface temperature (Joachimski *et al.* 2009, Brugger *et al.* 2019). • D – $\delta^{18}O$ (van Geldern 2004). • E – $\delta^{13}C$ (van Geldern 2004). • F – $^{87}Sr/^{86}Sr$ (van Geldern 2004). • G – $\delta^{11}B$ (Joachimski *et al.* 2005).

is some evidence for ocean acidification, although weak. In any case, finding evidence for the causality here is nearly impossible, and in particular, determining which environmental stressor had what effect in the respective organisms. When concerning calcifiers, a reduced investment into the calcified skeleton is intuitively linked to ocean acidification, but it is conceivable that a lower energetic investment in the skeleton may help to survive phases with other environmental stresses. Several of these environmental changes and potential stressors may have been regional, while others affected the whole hydrosphere.

Remarkably, the lowest septal slope factor is found in *Phoenixites* (0.0015) in the basal Famennian, right after the Kellwasser biotic crisis and thus following the anoxic conditions with low oceanic pH-levels. *Phoenixites* belongs to the suborder Tornoceratina together with *Mithraxites* from the Eifelian and *Sporadoceras* from the late Famennian; both *Mithraxites* and *Sporadoceras* have high adjusted septal slope factors (*Sporadoceras*: 0.0050, *Mithraxites*: 0.0062, the highest adjusted septal slope factor of all genera examined in this study). This is consistent with the results of Weber *et al.* (2022), according to whom a decrease in septal thickness followed a strong decline in oceanic pH-levels at the Triassic–Jurassic boundary. The results support the hypothesis of a positive selection for thin septa during ocean acidification events. Aside from this finding, Weber *et al.* (2022) discovered no significant correlation between the sea surface pH and the septal slope factor. This suggests that there is no major evolutionary trend for thinner septa during lower oceanic pH. Nevertheless, we hypothesize a threshold in oceanic pH, at which lower values do lead to a disadvantage in survival or reproduction of ammonoids with thicker septa. To confirm this hypothesis, more genera around the Kellwasser Event should be examined both within and outside the Tornoceratina suborder. Independent evidence comes from the abundance of dwarfed ammonoid faunas in the late Frasnian (Clausen 1969, Söte *et al.* 2021), opposed by extremely large gephuroceratids in other late Frasnian strata (Klug *et al.* 2025). This suggests that starvation may also have contributed to dwarfism and reduction of septal thickness (Otjacques *et al.* 2020). Additionally, more genera within the Tornoceratina from the Eifelian, Givetian, Frasnian and late Famennian need to be analysed, to infer if the trend of a decrease and increase of septal thickness around the Frasnian-Famennian boundary is truly present or only appears due to a small sample size of genera from that interval. The questions whether the observed pattern in sepatal thickness was caused by ocean acidification or other environmental factors and why septal thickness varied so strongly within tornoceratids can therefore not yet been answered definitely.

## Phylogeny

To test whether the phylogenetic relationship is reflected in the septal thickness, the adjusted septal slope factor was calculated for each genus and summarised for each taxonomic group at the order level for *Platyclymenia* and *Cymaclymenia* and at the suborder level for the other genera (Tab. 7). Each taxonomic group has a range of septal slope factors, which overlap to some extent, but still often show a similarity in septal thickness in closer related taxa. (Figs 11A, 12). However, there is one exception, the suborder Tornoceratina, where both the lowest (*Phoenixites*: 0.0015) and highest (*Mithraxites*: 0.0062) adjusted septal slope factors of all genera examined in this study were found. This high variation within a suborder is possibly due to repeated anoxic conditions during the late Frasnian (see previous chapter on Kellwasser and ocean acidification). Apart from the Tornoceratina, the variation within the taxonomic groups appears to be smaller than between the different groups, which implies some phylogenetic factor controlling septal thickness or similarities in conch shape influencing septal thickness. In addition to such relationships, the genera were grouped according to their time bins (Tab. 8, Figs 11B, 13). The highest variation in adjusted septal slope factors is found in the Eifelian. This seems to contradict the discussion above because relatively stable oceanic conditions are implied by a plateau in most abiotic factors during that time. However, some of the observed variation may be attributed to a greater taxonomic sample size during the Eifelian, at both the genus and suborder levels, and two global transgressive and anoxic events, which likely affected ammonoids as well (Choteč and Kačák events). Later time bins in particular are represented only by a small number of genera and only one or two suborders.

## Palaeolatitude

Weber *et al.* (2022) suggested a correlation between the septal slope factor and palaeolatitude, with ammonoids from higher latitudes having a smaller septal slope factor and thus thinner septa. This correlation would be explained by a causal link between ocean pH and septal thickness, since the cool sea water in high latitudes has a lower concentration of $CaCO_3$ than warmer seawater in lower latitudes, resulting in a greater effect of ocean acidification in high latitudes (Andersson *et al.* 2008, Weber *et al.* 2022). In this study all specimens originate from the Anti-Atlas of Morocco, with a palaeolatitude of approximately 40° south in the early Devonian (Fig. 14A) (Scotese 2001). Therefore, an analysis of the correlation between adjusted septal slope factor and palaeolatitude of contemporary species is not possible with our data. However, when

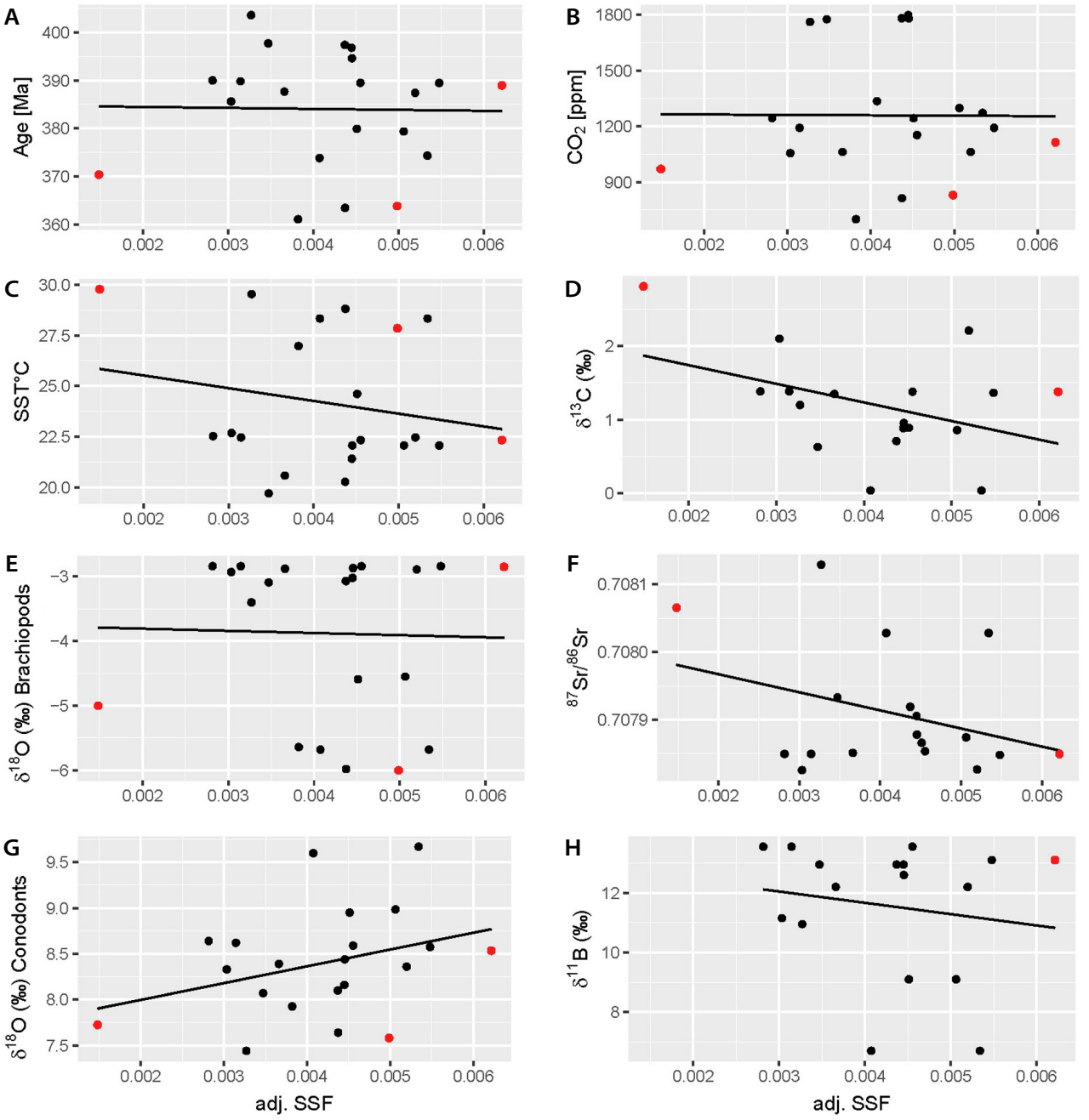


**Figure 16.** Correlation of age and abiotic factors (vertical axes) with adjusted septal slope factor (short: aSSF) (horizontal axis). Tornoceratids are marked in red (lowest aSSF value is *Phoenixites*, highest is *Mithraxites*). • A – age (Gradstein *et al.* 2020). • B – atmospheric $CO_2$ (Foster *et al.* 2017, Brugger *et al.* 2019). • C – isotopic sea surface temperature (Joachimski *et al.* 2009, Brugger *et al.* 2019). • D – $\delta^{13}C$ (van Geldern 2004). • E – $\delta^{18}O$ (van Geldern 2004). • F – $^{87}Sr/^{86}Sr$ (van Geldern 2004). • G – $\delta^{18}O$ from conodonts (Grossman & Joachimski 2020). • H – $\delta^{11}B$ (Joachimski *et al.* 2005).

combining the septal slope factors of the genera from this study with the data from Weber *et al.* (2022) and grouping the genera and species according to their palaeolatitude, it becomes apparent that the adjusted septal slope factors from this study fit in extremely well with their results of (Fig. 14B). This may also explain the lower variation of adjusted septal slope factors in the Devonian ammonoids, when compared with the Mesozoic ammonoids from Weber *et al.* (2022). To confirm the correlation of the septal thickness with palaeolatitude in the Devonian, specimens from localities with different palaeolatitudes would need to be examined. Nevertheless, our data support the pattern revealed by Weber *et al.* (2022) regarding correlation between the septal thickness and palaeolatitude.

## Conclusions

We studied the impact of atmospheric $CO_2$, sea surface temperature and oceanic pH on the septal thicknesses of Devonian ammonoids from the Anti-Atlas. We compared the distribution of septal thickness with isotopic proxy data ($\delta^{18}O$, $\delta^{13}C$, $\delta^{11}B$, $^{87}Sr/^{86}Sr$) from the literature representing seawater chemistry throughout the Devonian. Furthermore, we examined the variations in septal thickness within and between taxonomic groups. Our findings revealed significant differences in septal thickness among most lineages, indicating a phylogenetic signal and/ or similarity in conch morphology covarying with septal thickness. Within taxonomic groups, we found high similarities in relative septal thickness. However, one exception was discovered in *Phoenixites*, which has exceptionally thin septa. This genus occurred in the late Frasnian and early Famennian, *i.e*. in the strata that were deposited following the anoxia and possibly also phases of ocean acidification of the Kellwasser Events in the Late Devonian, contrasting with the thick septa of its older and younger relatives within the suborder Tornoceratina. This finding supports the hypothesis proposed by Weber *et al.* (2022) that reduced shell material could be an adaptive response to ocean acidification events or other environmental stressors (recently, this was suggested for brachiopods and forams by Wang *et al.* 2025). Although we did not find a significant correlation between septal thickness and long-term trends of atmospheric $CO_2$ or the examined isotopic proxy data, our results align with the research conducted by Weber *et al.* (2022) and provide further support for the correlation between septal thickness and palaeolatitude. Additional data would help to evaluate these relationships. These findings highlight the potential value of septal thickness in ammonoids as palaeoenvironmental proxies. To enhance the utility of these proxies and deepen our understanding of the interplay between phylogeny, palaeogeography, and ocean chemistry in shaping ammonoid shell morphology, future studies should incorporate the measurement of septal thickness in further taxa with a high stratigraphic resolution. Overall, we consider the study of septal thickness and related parameters as promising for palaeoenvironmental research, and hope that our results will inspire further investigations in this field.

## Acknowledgements

We greatly appreciate the working permits provided by the Ministère de l'Energie, des Mines, de l'Eau et de l'Environnement (Direction du Développement Minier, Division du Patrimoine, Rabat, Morocco). The Swiss National Science Foundation supported the research and field work (grant numbers 200021_149119, 200020_184894 and 205320_215642). AT was supported by the KAKENHI (grant number 24K17158). We thank the reviewers René Hoffmann (Bochum) and Kenneth De Baets (Warsaw) for their constructive criticism and input.

## References

Algeo, T.J., Scheckler, S.E. & Maynard, J.B. 2001. Effects of the Middle to Late Devonian spread of vascular land plants on weathering regimes, marine biotas, and global climate, 213–236. *In* Gensel, P.G. & Edwards, D. (eds) *Plants invade the land – evolutionary and environmental perspectives*. Columbia University Press. DOI 10.7312/gens11160-013

Andersson, A.J., Mackenzie, F.T. & Bates, N.R. 2008. implications of ocean acidification on Mg-calcite, high latitude and cold-water marine calcifiers. *Marine Ecology Progress Series 373*, 265–274. DOI 10.3354/meps07639

Bambach, R.K., Knoll, A.H. & Sepkoski, J.J., Jr. 2002. Anatomical and ecological constraints on Phanerozoic animal diversity in the marine realm. *Proceedings of the National Academy of Sciences 99(10)*, 6854–6859. DOI 10.1073/pnas.092150999

Barash, M.S. 2016. Causes of the great mass extinction of marine organisms in the Late Devonian. *Oceanology 56*, 863–875. DOI 10.1134/S0001437016050015

Barclay, K.M., Gingras, M.K., Packer, S.T. & Leighton, L.R. 2020. The role of gastropod shell composition and microstructure in resisting dissolution caused by ocean acidification. *Marine Environmental Research 162*, 105105. DOI 10.1016/j.marenvres.2020.105105

Beck, S.M., De Baets, K., Klug, C. & Korn, D. 2021. Analysis of septal spacing and septal crowding in Devonian and Carboniferous ammonoids. *Swiss Journal of Palaeontology 140(1)*, 1–21. DOI 10.1186/s13358-021-00235-x

Becker, R. & House, M.R. 1994. International Devonian goniatite zonation, Emsian to Givetian, with new records from Morocco. *Courier Forschungsinstitut Senckenberg 169*, 79–135.

Becker, R.T., Klug, C., Söte, T., Hartenfels, S., Aboussalam, Z.S. & El Hassani, A. 2019. The oldest ammonoids of Morocco (Tafilalt, lower Emsian). *Swiss Journal of Palaeontology 138*, 9–25. DOI 10.1007/s13358-019-00189-1

Becker, R.T., Marshall, J.E.A., Da Silva, A.-C., Agterberg, F.P., Gradstein, F.M. & Ogg, J.G. 2020. The Devonian Period, 733–810. *In* Gradstein, F.M., Ogg, J.G., Schmitz, M.D. & Ogg, G.M. (eds) *Geologic Time Scale 2020*. Elsevier. DOI 10.1016/B978-0-12-824360-2.00022-X

Belka, Z., Klug, C., Kaufmann, B., Korn, D., Döring, S., Feist, R. & Wendt, J. 1999. Devonian conodont and ammonoid succession of the eastern Tafilalt (Ouidane Chebbi section), Anti-Atlas, Morocco. *Acta Geologica Polonica 49*, 1–23.

Berner, R.A. & Kothavala, Z. 2001. Geocarb III: A revised model of atmospheric $CO_2$ over phanerozoic time. *American Journal of Science 301*, 182–204. DOI 10.2475/ajs.301.2.182

Berner, R., Maynard, J. & Scheckler, S. 1995. Late Devonian oceanic anoxic events and biotic crises: "Rooted" in the evolution of vascular plants. *GSA Today 5*, 45, 64–66.

Bijma, J., Spero, H.J. & Lea, D.W. 1999. Reassessing Foraminiferal Stable Isotope Geochemistry: Impact of the Oceanic Carbonate System (Experimental Results), 489–512. *In* Fischer, G. & Wefer, G. (eds) *Use of Proxies in Paleoceanography: Examples from the South Atlantic*. Springer, Berlin & Heidelberg. DOI 10.1007/978-3-642-58646-0_20

Boggild, O.B. 1930. The shell structure of the mollusks. *Det Kongelige Danske Videnskabernes Selskabs Skrifter, Natruvidenskabelig og Mathematisk, Afdeling, Ser. 9, 2*, 231–326.

Borges, F.O., Sampaio, E., Santos, C.P. & Rosa, R. 2023. Climate-change impacts on cephalopods: a meta-analysis. *Integrative and Comparative Biology 63(6)*, 1240–1265. DOI 10.1093/icb/icad102

Brugger, J., Hofmann, M., Petri, S. & Feulner, G., 2019. On the Sensitivity of the Devonian Climate to Continental Configuration, Vegetation Cover, Orbital Configuration, $CO_2$ Concentration, and Insolation. *Paleoceanography and Paleoclimatology 34*, 1375–1398. DOI 10.1029/2019PA003562

Buch, L. von 1832. Über Goniatiten. *Abhandlungen der Königlichen Akademie der Wissenschaften zu Berlin, Physikalische Klasse (for 1830)*, 159–187.

Carmichael, S.K., Waters, J.A., Suttner, T.J., Kido, E. & DeReuil, A.A. 2014. A new model for the Kellwasser Anoxia Events (Late Devonian): Shallow water anoxia in an open oceanic setting in the Central Asian Orogenic Belt. *Palaeogeography, Palaeoclimatology, Palaeoecology 399*, 394–403. DOI 10.1016/j.palaeo.2014.02.016

Clarkson, M.O., Kasemann, S.A., Wood, R.A., Lenton, T.M., Daines, S.J., Richoz, S., Ohnemueller, F., Meixner, A., Poulton, S.W. & Tipper, E.T. 2015. Ocean acidification and the Permo-Triassic mass extinction. *Science 348*, 229–232. DOI 10.1126/science.aaa0193

Clausen, C.-D. 1969. Oberdevonische Cephalopoden aus dem Rheinischen Schiefergebirge. II. Gephuroceratidae, Beloceratidae. *Palaeontographica, Abteilung A 132*, 95–178.

Cohen, A. & Holcomb, M. 2009. Why corals care about ocean acidification: uncovering the mechanism. *Oceanography 22*, 118–127. DOI 10.5670/oceanog.2009.102

Collins, M.J., Muyzer, G., Curry, G.B., Sandberg, P. & Westbroek, P. 1991. Macromolecules in brachiopod shells: characterization and diagenesis. *Lethaia 24*, 387–397. DOI 10.1111/j.1502-3931.1991.tb01491.x

De Baets, K. & Munnecke, A. 2018. Evidence for Palaeozoic orthoconic cephalopods with bimineralic shells. *Palaeontology 61(2)*, 173–181. DOI 10.1111/pala.12343

Dorey, N., Melzner, F., Martin, S., Oberhänsli, F., Teyssié, J.L., Bustamante, P., Gattuso, J.-P. & Lacoue-Labarthe, T. 2013. Ocean acidification and temperature rise: effects on calcification during early development of the cuttlefish *Sepia officinalis*. *Marine Biology 160(8)*, 2007–2022. DOI 10.1007/s00227-012-2059-6

Fligner, M.A. & Killeen, T.J. 1976. Distribution-Free Two-Sample Tests for Scale. *Journal of the American Statistical Association 71*, 210–213. DOI 10.1080/01621459.1976.10481517

Foster, G.L., Royer, D.L. & Lunt, D.J. 2017. Future climate forcing potentially without precedent in the last 420 million years. *Nature Communications 8*, *14845*. DOI 10.1038/ncomms14845

Ge, Y., Wang, H., Tian, Z., Zheng, D., Yi, L. & Han, H. 2022. Marine aragonite evolution in the oxygen-decreasing interval before the Cenomanian-Turonian Ocean anoxic event (OAE2) in the southeastern Neo-Tethys. *Sedimentary Geology 429*, 106078. DOI 10.1016/j.sedgeo.2021.106078

Geldern, R. van 2004. *Stabile Isotopenuntersuchungen an devonischen Brachiopoden*. 197 pp. Ph.D. thesis, Friedrich-Alexander-Universität, Erlangen-Nürnberg.

Geldern, R. van, Joachimski, M.M., Day, J., Jansen, U., Alvarez, F., Yolkin, E.A. & Ma, X.P. 2006. Carbon, oxygen and strontium isotope records of Devonian brachiopod shell calcite. *Palaeogeography, Palaeoclimatology, Palaeoecology 240*, 47–67. DOI 10.1016/j.palaeo.2006.03.045

Gradstein, F. & Ogg, J. 2004. *A Geologic Time Scale*. 589 pp. Cambridge University Press, Cambridge.

Gradstein, F.M. 2012. *The Geologic Time Scale 2012*. Elsevier, Amsterdam. DOI 10.1127/0078-0421/2012/0020

Gradstein, F.M., Ogg, J.G., Schmitz, M. & Ogg, G. 2020. *The Geologic Time Scale 2020*. Elsevier Science. DOI 10.1127/nos/2020/0634

Grossman, E.L. & Joachimski, M.M. 2020. Oxygen isotope stratigraphy, 279–307. *In* Gradstein, F.M., Ogg, J.G., Schmitz, M.D. & Ogg, G.M. (eds) *Geologic Time Scale 2020*. Elsevier. DOI 10.1016/B978-0-12-824360-2.00010-3

Gutowska, M.A., Pörtner, H.O. & Melzner, F. 2008. Growth and calcification in the cephalopod *Sepia officinalis* under elevated seawater $pCO_2$. *Marine Ecology Progress Series 373*, 303–309. DOI 10.3354/meps07782

Gutowska, M.A., Melzner, F., Pörtner, H.O. & Meier, S. 2010. Cuttlebone calcification increases during exposure to elevated seawater $pCO_2$ in the cephalopod *Sepia officinalis*. *Marine Biology 157(7)*, 1653–1663. DOI 10.1007/s00227-010-1438-0

Hahn, S., Griesshaber, E., Schmahl, W.W., Neuser, R.D., Ritter, A.C., Hoffmann, R. & Immenhauser, A. 2014. Exploring aberrant bivalve shell ultrastructure and geochemistry as proxies for past sea water acidification. *Sedimentology 61(6)*, 1625–1658. DOI 10.1111/sed.12107

Hautmann, M. 2004. Effect of End-Triassic $CO_2$ maximum on carbonate sedimentation and marine mass extinction. *Facies 50*, 257–261. DOI 10.1007/s10347-004-0020-y

Hautmann, M. 2006. Shell mineralogical trends in epifaunal Mesozoic bivalves and their relationship to seawater chemistry and atmospheric carbon dioxide concentration. *Facies 52*, 417–433. DOI 10.1007/s10347-005-0029-x

Hautmann, M., Benton, M. & Tomašových, A. 2008. Catastrophic ocean acidification at the Triassic-Jurassic

boundary. *Neues Jahrbuch für Geologie und Paläontologie. Abhandlungen 249*, 119–127.
DOI /10.1127/0077-7749/2008/0249-0119

Helsel, D. & Frans, L. 2006. A Regional Kendall Test for Trend. *Environmental Science & Technology 40*, 4066–4073. DOI 10.1021/es051650b

Hewitt, R.A. & Stait, B. 1988. Seasonal variation in septal spacing of Sepia officinalis and some Ordovician actinocerid nautiloids. *Lethaia 21(4)*, 383–394.
DOI 10.1111/j.1502-3931.1988.tb01767.x

Hönisch, B., Ridgwell, A., Schmidt, D.N., Thomas, E., Gibbs, S.J., Sluijs, A., Zeebe, R., Kump, L., Martindale, R.C., Greene, S.E., Kiessling, W., Ries, J., Zachos, J.C., Royer, D.L., Barker, S., Marchitto, T.M. Jr., Moyer, R., Pelejero, C., Ziveri, P., Foster, G.L. & Williams, B. 2012. The geological record of ocean acidification. *Science 335(6072)*, 1058–1063. DOI 10.1126/science.1208277

Immenhauser, A., Schöne, B., Hoffmann, R. & Hachenberg, A. 2016. Mollusc and brachiopod skeletal hard parts: Intricate archives of their marine environment. *Sedimentology 63*, 1–59. DOI 10.1111/sed.12231

Janiszewska, K., Mazur, M., Machalski, M. & Stolarski, J. 2018. From pristine aragonite to blocky calcite: Exceptional preservation and diagenesis of cephalopod nacre in porous Cretaceous limestones. *Plos One 13(12)*, e0208598.
DOI 10.1371/journal.pone.0208598

Joachimski, M.M., Simon, L., Geldern, R. van & Lécuyer, C. 2005. Boron isotope geochemistry of Paleozoic brachiopod calcite: Implications for a secular change in the boron isotope geochemistry of seawater over the Phanerozoic. *Geochimica et Cosmochimica Acta 69*, 4035–4044.
DOI 10.1016/j.gca.2004.11.017

Joachimski, M.M., Breisig, S., Buggisch, W., Talent, J.A., Mawson, R., Gereke, M., Morrow, J.R., Day, J. & Weddige, K. 2009. Devonian climate and reef evolution: Insights from oxygen isotopes in apatite. *Earth and Planetary Science Letters 284*, 599–609. DOI 10.1016/j.epsl.2009.05.028

Jurikova, H., Liebetrau, V., Gutjahr, M., Rollion-Bard, C., Hu, M.Y., Krause, C., Henkel, D., Hiebenthal, C., Schmidt, M., Laudien, J. & Eisenhauer, A. 2019. Boron isotope systematics of cultured brachiopods: Response to acidification, vital effects and implications for palaeo-pH reconstruction. *Geochimica et Cosmochimica Acta 248*, 370–386. DOI 10.1016/j.gca.2019.01.015

Kaplan, M.B., Mooney, T.A., McCorkle, D.C. & Cohen, A.L. 2013. Adverse effects of ocean acidification on early development of squid (*Doryteuthis pealeii*). *PLoS One 8(5)*, e63714. DOI 10.1371/journal.pone.0063714

Kiessling, W. & Simpson, C. 2011. On the potential for ocean acidification to be a general cause of ancient reef crises. *Global Change Biology 17*, 56–67.
DOI 10.1111/j.1365-2486.2010.02204.x

Kiessling, W., Reddin, C.J., Dowding, E.M., Dimitrijević, D., Raja, N.B. & Kocsis, Á.T. 2025. Marine biological responses to abrupt climate change in deep time. *Paleobiology, 51*, 97–111. DOI 10.1017/pab.2024.20

Klug, C. 2001. Early Emsian ammonoids from the eastern Anti-Atlas (Morocco) and their succession. *Paläontologische Zeitschrift 74*, 479–515. DOI 10.1007/BF02988158

Klug, C. 2002. Quantitative stratigraphy and taxonomy of late Emsian and Eifelian ammonoids of the Anti-Atlas (Morocco). *CFS Courier Forschungsinstitut Senckenberg 238*, 1–109.

Klug, C., Korn, D., De Baets, K., Kruta, I. & Mapes, R.H. (eds) 2015a. *Ammonoid paleobiology, Volume I: from anatomy to ecology*, 1–947. *Topics in Geobiology*. Springer, Dordrecht. DOI 10.1007/978-94-017-9630-9

Klug, C., Kröger, B., Vinther, J., Fuchs, D. & De Baets, K. 2015b. Ancestry, origin and early evolution of ammonoids, 3–24. *In* Klug, C., Korn, D., De Baets, K., Kruta, I. & Mapes, R.H. (eds) *Ammonoid Paleobiology: From Macroevolution to Paleogeography*. Springer, Dordrecht. DOI 10.1007/978-94-017-9633-0_1

Klug, C., Fuchs, D., Pohle, A., Korn, D., De Baets, K., Hoffmann, R., Ware, D. & Ward 2025. Cephalopod body size and macroecology through deep time. *Scientific Reports 15(30736)*, 1–16.
DOI 10.1038/s41598-025-13940-1

Korn, D. 1999. Famennian ammonoid stratigraphy of the Ma'der and Tafilalt (Eastern Anti-Atlas, Morocco). *Abhandlungen der Geologischen Bundesanstalt 54*, 147–179.

Korn, D. 2001. Morphometric evolution and phylogeny of Paleozoic ammonoids. Early and Middle Devonian. *Acta Geologica Polonoca 51*, 193–215.

Korn, D. & Klug, C. 2002. *Ammoneae Devonicae*, 1–375. *In* Riegraf, W. (ed.) *In Fossilium Catalogus 1: Animalia.* (Backhuys) Leiden.

Korn, D. & Klug, C. 2015. Paleozoic Ammonoid Biostratigraphy, 299–328. *In* Klug, C., Korn, D., De Baets, K., Kruta, I. & Mapes, R.H. (eds) *Ammonoid Paleobiology: From Macroevolution to Paleogeography*. Springer, Dordrecht. DOI 10.1007/978-94-017-9633-0_12

Korn, D., Klug, C. & Walton, S.A. 2015. Taxonomic Diversity and Morphological Disparity of Paleozoic Ammonoids, 431–464. *In* Klug, C., Korn, D., De Baets, K., Kruta, I. & Mapes, R.H. (eds) *Ammonoid Paleobiology: From Macroevolution to Paleogeography.* Springer, Dordrecht. DOI 10.1007/978-94-017-9633-0_16

Korn, D., Klug, C. & Reisdorf, A. 2000. Middle Famennian Ammonoid Stratigraphy in the Amessoui Syncline (Late Devonian; Eastern Anti-Atlas, Morocco). *Travaux de l'Institut Scientifique (Rabat), Série Géologie & Géographie Physique 20*, 69–77.

Kraft, S., Korn, D. & Klug, C. 2008. Patterns of ontogenetic septal spacing in Carboniferous ammonoids. *Neues Jahrbuch für Geologie und Paläontologie, Abhandlungen 250(1)*, 31–44. DOI 10.1127/0077-7749/2008/0250-0031

Kruta, I., Landman, N.H. & Cochran, J.K. 2014. A new approach for the determination of ammonite and nautilid habitats. *PLoS One 9(1)*, e87479.
DOI 10.1371/journal.pone.0087479

Kump, L.R., Bralower, T.J. & Ridgwell, A. 2009. Ocean acidification in deep time. *Evolving Earth 22*, 94–107.
DOI 10.5670/oceanog.2009.100

Land, L.S. & Leo Lynch, F. 1996. $\delta^{18}O$ values of mudrocks:

More evidence for an $^{18}O$-buffered ocean. *Geochimica et Cosmochimica Acta 60*, 3347–3352. DOI 10.1016/0016-7037(96)00185-8

Maneja, R., Piatkowski, U. & Melzner, F. 2011. Effects of ocean acidification on statolith calcification and prey capture in early life cuttlefish, *Sepia officinalis*. *Journal of Shellfish Research 30(3)*, 1011.

Marshall, J., Astin, T., Tel'nova, O.P. & Gaca 2025. Terrestrial palaeoclimate, mercury, atmospheric CO2 and land plants through the Late Devonian mass extinction. *Abstracts of GeoTolosa 2025*, 32. DOI 10.1144/jgs2024-187

McGhee, G.R. Jr., Clapham, M.E., Sheehan, P.M., Bottjer, D.J. & Droser, M.L. 2013. A new ecological-severity ranking of major Phanerozoic biodiversity crises. *Palaeogeography, Palaeoclimatology, Palaeoecology 370*, 260–270. DOI 10.1016/j.palaeo.2012.12.019

Menning, M. & Hendrich, A. 2002. *Stratigraphische Tabelle von Deutschland 2002*. Deutsche Stratigraphische Kommission, Potsdam (GeoForschungsZentrum), Forschungsinstitut Senckenberg, Frankfurt a. M.

Monnet, C., Klug, C., Goudemand, N., De, K. & Bucher, H. 2011. Quantitative biochronology of Devonian ammonoids from Morocco and proposals for a refined unitary association method. *Lethaia 44*, 469–489. DOI 10.1111/j.1502-3931.2010.00256.x

Morse, J.W. & Mackenzie, F.T. 1990. *Geochemistry of Sedimentary Carbonates*. 706 pp. Elsevier, Amsterdam.

Muehlenbachs, K. 1998. The oxygen isotopic composition of the oceans, sediments and the seafloor. *Chemical Geology 145*, 263–273. DOI 10.1016/S0009-2541(97)00147-2

Münster, G. Graf zu 1832. *Ueber die Planuliten und Goniatiten im Uebergangs-Kalk des Fichtelgebirges*. 38 pp. Birner, Bayreuth.

Nätscher, P.S., Dera, G., Reddin, C.J., Rita, P. & De Baets, K. 2021. Morphological response accompanying size reduction of belemnites during an Early Jurassic hyperthermal event modulated by life history. *Scientific Reports 11(1)*, 14480. DOI 10.1038/s41598-021-93850-0

Otjacques, E., Repolho, T., Paula, J.R., Simão, S., Baptista, M. & Rosa, R. 2020. Cuttlefish buoyancy in response to food availability and ocean acidification. *Biology 9(7)*, 147. DOI 10.3390/biology9070147

Palmer, A.R. 1992. Calcification in marine molluscs: how costly is it? *Proceedings of the National Academy of Sciences 89*, 1379–1382. DOI 10.1073/pnas.89.4.1379

Penman, D.E., Hönisch, B., Rasbury, E.T., Hemming, N.G. & Spero, H.J. 2013. Boron, carbon, and oxygen isotopic composition of brachiopod shells: Intra-shell variability, controls, and potential as a paleo-pH recorder. *Chemical Geology 340*, 32–39. DOI 10.1016/j.chemgeo.2012.11.016

Pohle, A., Hoffamann, R, Nützel, A., Seuss, B., Aubrechtová, M., Kröger, B., Stevens, K. & Immenhauser, A. 2025. Microstructural and geochemical evidence offers a solution to the cephalopod cameral deposits riddle. *Palaeontology 68(6)*, e70032. DOI 10.1111/pala.70032

Rakocinski, M., Kucharczyk, J., Pisarzowska, A. & Zaton, M. 2023. Redox changes and mercury signature during the Lower Alum Shale Event (mid-Tournaisian, Mississippian) in the Rhenish Massif: Implications for oxygenation history and volcanism in southern Laurussian shelf and Palaeotethys Ocean. *Global and Planetary Change 227*, 1–19. DOI 10.1016/j.gloplacha.2023.104165

Rasbury, E.T. & Hemming, N.G. 2017. Boron isotopes: A "Paleo-pH Meter" for tracking ancient atmospheric $CO_2$. *Elements 13(4)*, 243–248. DOI 10.2138/gselements.13.4.243

Ridgwell, A. & Zeebe, R.E. 2005. The role of the global carbonate cycle in the regulation and evolution of the Earth system. *Earth and Planetary Science Letters 234*, 299–315. DOI 10.1016/j.epsl.2005.03.006

Rouam, S. 2013. False Discovery Rate (FDR), 731–732. *In* Dubitzky, W., Wolkenhauer, O., Cho, K.-H. & Yokota, H. (eds) *Encyclopedia of Systems Biology*. Springer, New York. DOI 10.1007/978-1-4419-9863-7_223

Salifu, M., Aiglsperger, T., Hällström, L., Martinsson, O., Billström, K., Ingri, J., Dold, B. & Alakangas, L. 2018. Strontium ($^{87}Sr/^{86}Sr$) isotopes: A tracer for geochemical processes in mineralogically-complex mine wastes. *Applied Geochemistry 99*, 42–54. DOI 10.1016/j.apgeochem.2018.10.022

Sandoval, J., O'Dogherty, L. & Guex, J. 2001. Evolutionary Rates of Jurassic Ammonites in Relation to Sea-Level Fluctuations. *Palaios 16*, 311–335. DOI 10.1669/0883-1351(2001)016<0311:EROJAI>2.0.CO;2

Scotese, C. 2001. *Atlas of Earth History, Volume 1*. 52 pp. Paleogeography, PALEOMAP Project, Arlington, Texas.

Shapiro, S.S. & Wilk, M. 1965. An analysis of variance test for normality (complete samples)†. *Biometrika 52*, 591–611. DOI 10.1093/biomet/52.3-4.591

Simonet Roda, M., Griesshaber, E., Ziegler, A., Rupp, U., Yin, X., Henkel, D., Häussermann, V., Laudien, J., Brand, U., Eisenhauer, A., Checa, A.G. & Schmahl, W.W. 2019. Calcite fibre formation in modern brachiopod shells. *Scientific Reports 9*, 598. DOI 10.1038/s41598-018-36959-z

Söte, T., Becker, R.T., Herd, K.J. & Bockwinkel, J. 2021. Upper Frasnian Tornoceratidae (Ammonoidea) from the Sand Formation (Bergisch Gladbach-Paffrath Syncline, Rhenish Massif). *Paläontologische Zeitschrift 95*, 1–37. DOI 10.1007/s12542-020-00546-3

Spearman, C. 1904. The proof and measurement of association between two things. *The American Journal of Psychology 15*, 72–101. DOI 10.2307/1412159

Streel, M., Caputo, M. V, Loboziak, S. & Melo, J.H.G. 2000. Late Frasnian–Famennian climates based on palynomorph analyses and the question of the Late Devonian glaciations. *Earth-Science Reviews 52*, 121–173. DOI 10.1016/S0012-8252(00)00026-X

Tajika, A., Landman, N. H., Cochran, J. K., Nishida, K., Shirai, K., Ishimura, T., Murakami-Sugihara, N. & Sato, K. 2023. Ammonoid extinction versus nautiloid survival: Is metabolism responsible? *Geology 51(7)*, 621–625. DOI 10.1130/G51116.1

Tajika, A., Nützel, A. & Klug, C. 2018. The old and the new plankton: ecological replacement of associations of mollusc plankton and giant filter feeders after the Cretaceous? *PeerJ 6*, e4219. DOI 10.7717/peerj.4219

Tajika, A., Landman, N.H., Hoffmann, R., Lemanis, R., Morimoto, N., Ifrim, C. & Klug, C. 2020. Chamber volume development, metabolic rates, and selective extinction in cephalopods. *Scientific Reports 10*, 2950. DOI 10.1038/s41598-020-59748-z

Torsvik, T.H., Cocks, L.R.M., Domeier, M., Marcilly, C.M. & Dowding, E.M. 2025. Devonian palaeogeography and environmental change: an incomplete chronicle. *Zeitschrift der Deutschen Gesellschaft für Geowissenschaften 176(2)*, 193–214. DOI 10.1127/zdgg/2025/0454

Trecalli, A., Spangenberg, J., Adatte, T., Föllmi, K.B. & Parente, M. 2012. Carbonate platform evidence of ocean acidification at the onset of the early Toarcian oceanic anoxic event. *Earth and Planetary Science Letters 357*, 214–225. DOI 10.1016/j.epsl.2012.09.043

Veizer, J., Bruckschen, P., Pawellek, F., Diener, A., Podlaha, O.G., Carden, G.A.F., Jasper, T., Korte, C., Strauss, H., Azmy, K. & Ala, D. 1997. Oxygen isotope evolution of Phanerozoic seawater. *Palaeogeography, Palaeoclimatology, Palaeoecology 132*, 159–172. DOI 10.1016/S0031-0182(97)00052-7

Veizer, J., Ala, D., Azmy, K., Bruckschen, P., Buhl, D., Bruhn, F., Carden, G.A.F., Diener, A., Ebneth, S., Godderis, Y., Jasper, T., Korte, C., Pawellek, F., Podlaha, O.G. & Strauss, H. 1999. $^{87}Sr/^{86}Sr$, $\delta^{13}C$ and $\delta^{18}O$ evolution of Phanerozoic seawater. *Chemical Geology 161*, 59–88. DOI 10.1016/S0009-2541(99)00081-9

Villier, L. & Korn, D. 2004. Morphological Disparity of Ammonoids and the Mark of Permian Mass Extinctions. *Science 306*, 264–266. DOI 10.1126/science.1102127

Wang, F., Finnegan, S., Dal Corso, J., Ye, F., Wu, Y., Jing Chen, Jiang, S., Tian, L., Dai, X., Chu, D., Song, H., Tong, J. & Song, H. 2025. Brachiopods and forams reduced calcification costs through morphological simplification during mass extinction events. *Nature Ecology & Evolution 9*, 1456–1468. DOI 10.1038/s41559-025-02749-w

Weber, C., Hautmann, M., Tajika, A. & Klug, C. 2022. Is the relative thickness of ammonoid septa influenced by ocean acidification, phylogenetic relationships and palaeogeographic position? *Swiss Journal of Palaeontology 141*, 1–26. DOI 10.1186/s13358-022-00246-2